INTERNATIONAL JOURNAL FOR NUMERICAL METHODS IN ENGINEERING
Int. J. Numer. Meth. Engng 2010; **83**:1081–1113
Published online 31 March 2010 in Wiley InterScience (www.interscience.wiley.com). DOI: 10.1002/nme.2879

Ghost forces and spurious effects in atomic-to-continuum coupling methods by the Arlequin approach

Ludovic Chamoin[1], Serge Prudhomme[2], H. Ben Dhia[3] and Tinsley Oden[2,*,†]

[1]*LMT, Ecole Normale Supérieure de Cachan, 61 Avenue du Président Wilson, Cachan Cedex 94235, France*
[2]*Institute for Computational Engineering and Sciences, The University of Texas at Austin, 1 University Station C0200, Austin, TX 78712, U.S.A.*
[3]*Laboratoire de Mécanique des Sols, Structures et Matériaux, Ecole Centrale de Paris, 1 Grande Voie des Vignes, Chatenay-Malabry Cedex 92295, France*

SUMMARY

The main objective of this work is to identify spurious effects and propose a corrective method when coupling a particle model involving long–range interaction potentials with a first gradient homogenized model using the Arlequin framework. The most significant spurious effects are generally created by the so-called ghost forces that arise in coupling methods based on the minimization of a global energy functional. They depend as well on the coupling formulation itself, on the notion of representative volume element, and on the discretization of the continuum model. The proposed corrective technique is based on post-processing of the approximate solution by introducing dead forces that can be systematically evaluated and consistently inserted within the Arlequin formulation. Efficiency of the corrective procedure is demonstrated on 1D and 2D examples. Copyright © 2010 John Wiley & Sons, Ltd.

Received 9 September 2009; Revised 11 December 2009; Accepted 8 January 2010

KEY WORDS: Arlequin framework; global energy minimization; dead forces; corrective method

1. INTRODUCTION

Computer simulations at the atomic scale have drawn the attention of many scientists during the last decade [1–4] due to advances in nanotechnologies and the need to access fine-scale details in the simulation of nanoprocesses. Needless to say, fully molecular computations are yet out of reach with current computing resources, as realistic applications of engineering interest would require an excessive number of degrees of freedom. To circumvent this issue, multiscale approaches have

*Correspondence to: Tinsley Oden, Institute for Computational Engineering and Sciences, The University of Texas at Austin, 1 University Station C0200, Austin, TX 78712, U.S.A.
†E-mail: oden@ices.utexas.edu

Contract/grant sponsor: U.S. Department of Energy Multiscale Mathematics Program; contract/grant number: DE-G02-05ER25701

been advanced in recent years that allow to significantly reduce the size of such problems. To name a few, one can list the handshake method [5], the bridging-scale method [6], or the bridging-domain method [7], which can be viewed as an extension of the Arlequin framework proposed in [8]. Another class of multiscale methods for blending particle and continuum scales is that produced by the quasi-continuum approach [9, 10]; however, this class of methods can be viewed as model reduction (or coarsening) methods rather than genuine coupling methods. More recently, another atomic-to-continuum coupling method based on the Arlequin framework has been developed for the simulation of polymerization processes [3, 11–14]. In the static regime, the latter enforces in the overlap zone the equality between the continuum displacement and an interpolation of the atomistic one by means of a H^1-type coupling (rather than the L^2-type used in the bridging-domain method, as it was shown in [11] that only the former does yield a well-posed problem, see also [15] for clarifying comments). Moreover, the partition of energy is adapted to cope with the discrete character of the atomistic model. The Arlequin framework actually provides an attractive method for blending highly heterogeneous atomic models with continuum models as it does not assume that the so-called Cauchy–Born hypothesis be satisfied. We note that the standard bridging-domain method has recently been modified in [16] to be able to deal with composite materials. The authors considered in the paper periodic structures for which they identify primary and secondary sublattices. Only the primary particles are then constrained on the overlap region following the Cauchy–Born rule and the secondary particles are let free with respect to the continuum solution.

Coupling methods for atomic-to-continuum simulations may exhibit spurious effects in the vicinity of the coupling region that may result in inaccurate numerical solutions. Spurious effects are for example those induced by so-called ghost forces which were first observed in the context of the quasi-continuum method [17] and numerical corrective methods [18–21] have since then been proposed that modify the original version of the quasi-continuum method in order to reduce these effects. The objective of the present paper is to analyze the sources and magnitude of spurious effects for atomic-to-continuum coupling methods based on the Arlequin framework [7, 11, 12, 22] and to propose corrective techniques, if necessary, to reduce their influence. For example, as in the quasi-continuum method, we show that the Arlequin formulation is not immune against the presence of ghost forces. It has also been observed that spurious effects in Arlequin-type coupling may arise from a local loss of coercivity of the method [15]. We propose here a corrective method that involves the introduction of extra forces that can be automatically calculated from the current state of the particle and continuum displacements. These extra forces are added to the Arlequin formulation by means of a partition of unity and iteratively updated until convergence through an iterative procedure. This correction technique leads to significant improvements of the Arlequin coupled solution when applied to one-dimensional and two-dimensional numerical examples. We also analyze the effect of the corrective method in the case when an adaptive Arlequin approach [13] would be considered. The question is whether it is more efficient to simply enlarge the molecular region in order to decrease the influence of the spurious effects on the accuracy of local quantities of interest or to employ the corrective method at an extra cost.

The paper is organized as follows. We present in Section 2 the particle and continuum models. The Arlequin framework is briefly reviewed in Section 3. Section 4 is devoted to the description of the various sources of the spurious effects encountered in the Arlequin method. The proposed corrective method to control the spurious effects is introduced in Section 5 and its efficiency is demonstrated on numerical examples in Section 6. Concluding remarks are provided in Section 7.

DOI: 10.1002/nme

2. PARTICLE AND CONTINUUM MODELS

2.1. Particle model problem

We consider a domain Ω in $\mathbb{R}^d$, $d=1$, 2, or 3, which represents a structure modeled at the particle scale (see Figure 1). The structure consists of a set of N_p particles connected to each other by means of interatomic potentials. The initial position of particle i, i.e. its position in the unloaded configuration, is defined by vector $\mathbf{x}_i$, $i=1,\ldots,N_p$. The system of particles in Ω is subjected to pointwise forces $\mathbf{f}_i$ applied to each particle i, $1\leqslant i\leqslant N_p$. We also suppose that $N_D<N_p$ particles are subjected to Dirichlet boundary conditions. The new position of particle i in the deformed configuration is defined by vector $\mathbf{r}_i\in\mathbb{R}^d$. The displacement of the particles is conveniently represented in compact form by means of vector $\mathbf{z}=[\mathbf{z}_1,\mathbf{z}_2,\ldots,\mathbf{z}_{N_p}]\in\mathbb{R}^{d\times N_p}$, where $\mathbf{z}_i=\mathbf{r}_i-\mathbf{x}_i$. Throughout the paper, pairwise interactions between particles are modeled by harmonic potentials V_{ij}:

$$V_{ij}(\mathbf{z}_i,\mathbf{z}_j)=\tfrac{1}{2}k_{ij}(r_{ij}-r_{ij}^0)^2 \tag{1}$$

where r_{ij}^0 is the equilibrium distance between particle i and particle j (we assume here that the initial configuration is at equilibrium, i.e. $r_{ij}^0=|\mathbf{x}_j-\mathbf{x}_i|$), r_{ij} is the current distance between particle i and particle j (i.e. $r_{ij}=|\mathbf{r}_j-\mathbf{r}_i|=|\mathbf{x}_j+\mathbf{z}_j-\mathbf{x}_i-\mathbf{z}_i|$), and k_{ij} is a positive stiffness coefficient. The global strain energy of the system is then given by:

$$E(\mathbf{z})=\sum_{i=1}^{N_p}\sum_{j=i+1}^{N_p}V_{ij}(\mathbf{z}_i,\mathbf{z}_j)=\frac{1}{2}\sum_{i=1}^{N_p}\sum_{j=1}^{N_p}V_{ij}(\mathbf{z}_i,\mathbf{z}_j) \tag{2}$$

The energy of the system is often approximated by introducing a cut-off distance around each particle i. We then restrict interactions to a set $\mathcal{N}_i$ of particles located in a neighborhood of particle i such that:

$$E(\mathbf{z})=\frac{1}{2}\sum_{i=1}^{N_p}\sum_{j\in\mathcal{N}_i}V_{ij}(\mathbf{z}_i,\mathbf{z}_j) \tag{3}$$

We denote by $\mathscr{Z}_D$ the set of admissible displacements, that is, the subset of $\mathbb{R}^{d\times N_p}$ made of the displacements that verify the Dirichlet boundary conditions, and by $\mathscr{Z}_0$ the subset of displacements in $\mathbb{R}^{d\times N_p}$ that vanish on the Dirichlet boundary. The displacement $\mathbf{y}$ is then obtained by solving the minimization problem:

$$\mathbf{y}=\operatorname*{argmin}_{\mathbf{z}\in\mathscr{Z}_D}W_p(\mathbf{z}) \tag{4}$$

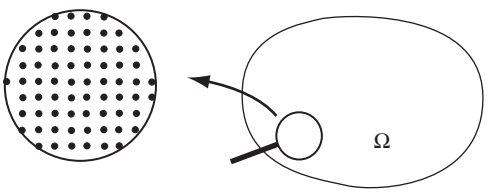

Figure 1. The particle domain Ω.

DOI: 10.1002/nme

where W_p is the potential energy of the system:

$$W_p(\mathbf{z}) = E(\mathbf{z}) - \sum_{i=1}^{N_p} \mathbf{f}_i \cdot \mathbf{z}_i \tag{5}$$

By differentiation, the weak form of problem (4) becomes:

$$\boxed{\text{Find } \mathbf{y} \in \mathscr{Z}_D \text{ such that } B(\mathbf{y};\mathbf{z}) = F(\mathbf{z}) \quad \forall \mathbf{z} \in \mathscr{Z}_0} \tag{6}$$

where the semilinear form $B(\cdot;\cdot)$ and linear form $F(\cdot)$ are defined as:

$$\begin{aligned} B(\mathbf{y};\mathbf{z}) &= \sum_{i=1}^{N_p} \frac{\partial E(\mathbf{y})}{\partial \mathbf{y}_i} \cdot \mathbf{z}_i \\ F(\mathbf{z}) &= \sum_{i=1}^{N_p} \mathbf{f}_i \cdot \mathbf{z}_i \end{aligned} \tag{7}$$

As a model example, we shall consider throughout this work a simple 1D particle structure. The domain $\Omega \subset \mathbb{R}$ is made of N_p particles, separated by length ℓ in the unloaded configuration, so that

$$x_i - x_{i-1} = \ell, \quad \forall i = 2, \ldots, N_p \tag{8}$$

We assume in this paper that the chain of particles is held fixed at x_1 with prescribed displacement $y_{1,D} = 0$, in which case $\mathscr{Z}_D = \mathscr{Z}_0$. Using above notations, (4) or (6) lead to the system of equations:

$$\sum_{j \in \mathscr{N}_i} k_{ij}(y_i - y_j) = f_i, \quad \forall i = 2, \ldots, N_p \tag{9}$$

where $\mathscr{N}_i = \{i - M_i, \ldots, i-1, i+1, \ldots, i+M_i\}$ is the set of neighbors around particle i that lie within the cut-off distance for the calculation of the interaction potentials. In the following, we only consider the case where M_i is the same for all particles, i.e. $M_i = M$, $i = 1, \ldots, N_p$. The definition of $\mathscr{N}_i$ is of course adjusted for those particles in the vicinity of the boundaries of Ω.

2.2. Homogenization and continuum model

The minimization problem (4) or (6) usually becomes intractable for large numbers of particles. However, we believe that the calculation of specific quantities of the solution can be accurately approximated by replacing the particle model by a coarser model (e.g. continuum model) in a subregion $\Omega_c \subset \Omega$ away from the region of interest. In doing so, the role of the continuum model is to propagate only the large-scale information through Ω_c. The choice of this continuum model depends on the nature of the material but should be selected as a 'compatible' model with the particle model in some homogenization sense.

We suppose in this section that the loading of the particles is such that only 'large-scale' displacements are observable in the whole domain Ω. We then describe how the particle model can be replaced in Ω by a continuum model that is derived from the former. The main idea is to replace the discrete displacement $\mathbf{y}$ by a continuous field $\mathbf{u} = \hat{\mathbf{X}} - \mathbf{X}$, where $\mathbf{X}$ and $\hat{\mathbf{X}}$ represent the

DOI: 10.1002/nme

initial and current position of a point in Ω. We then introduce a strain energy density ω^c so that the global strain energy in the continuum region Ω reads

$$E^c = E^c(\mathbf{u}) = \int_\Omega \omega^c(\mathbb{F}(\mathbf{u}))\,\mathrm{d}X \tag{10}$$

where $\mathbb{F} = \partial\hat{\mathbf{X}}/\partial\mathbf{X} = \mathbb{I} + \nabla_{\mathbf{X}}\mathbf{u}$ is the deformation gradient tensor. Selecting here linear elasticity as our continuum model, assuming small deformations, and a linearly elastic material, the strain energy density ω^c is given by:

$$\omega^c = \omega^c(\mathbf{u}) = \tfrac{1}{2}\mathbf{C}\varepsilon(\mathbf{u}) : \varepsilon(\mathbf{u}), \quad \varepsilon(\mathbf{u}) = \tfrac{1}{2}(\nabla\mathbf{u} + \nabla^{\mathrm{T}}\mathbf{u}) \tag{11}$$

where $\mathbf{C}$ is the Hooke tensor and ε the linearized strain tensor. Other forms of strain energy, depending on material behaviors (hyperelasticity, viscoelasticity, etc.), could alternatively be employed (for instance, a Mooney–Rivlin material is considered in [3]).

The homogenized continuum model is obtained by assuming a specific form for $\mathbf{C}$ based on macroscopic properties of the particle network (isotropy, orthotropy, etc.) and calibrating the corresponding parameters using local measurements of the particle strain energy. When the Cauchy–Born rule is assumed to hold, the density ω^c can be straightforwardly derived by interpolating the displacements of the interior particles of an infinite structure subjected to a uniform deformation gradient $\mathbb{F}$. The density ω^c then corresponds to the averaged strain energy over a given volume of the material. However, in cases where the Cauchy–Born rule is known not to hold, we resort to the concept of Representative Volume Element (RVE): a macroscopic deformation gradient is applied to the boundary of the RVE and the associated strain energy E^c is numerically computed solving the particle model, from which the strain energy density ω^c is estimated. These two approaches are illustrated on a 1D structure, for which we consider four cases (see Figure 2):

1. In the first two cases, bond stiffness coefficients are assumed uniform and the unit cell is taken of length ℓ. In Case 1, only nearest neighbor interactions are considered (cut-off distance

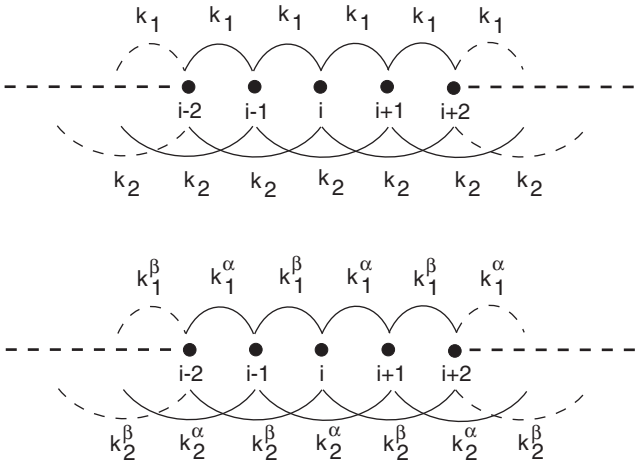

Figure 2. Configurations of the interatomic potentials: Cases 1 and 2 represented by bond stiffnesses k_1 and/or k_2 (top), Cases 3 and 4 represented by bond stiffnesses (k_1^α, k_1^β) and/or (k_2^α, k_2^β) (bottom).

DOI: 10.1002/nme

Table I. Equivalent Young's modulus obtained with Methods 1 and 2 for the four cases considered.

	Case 1	Case 2	Case 3	Case 4
Cauchy–Born rule approach	$k_1\ell$	$(k_1+4k_2)\ell$	$\frac{k_1^\alpha+k_1^\beta}{2}\ell$	$(\frac{k_1^\alpha+k_1^\beta}{2}+2k_2^\alpha+2k_2^\beta)\ell$
RVE approach	$k_1\ell$	$(k_1+4k_2)\ell$	$\frac{2k_1^\alpha k_1^\beta}{k_1^\alpha+k_1^\beta}\ell$	$(\frac{2k_1^\alpha k_1^\beta}{k_1^\alpha+k_1^\beta}+2k_2^\alpha+2k_2^\beta)\ell$

equal to ℓ, i.e. $M=1$), with inter-atomic stiffness equal to k_1. In Case 2, both nearest and next-nearest neighbor interactions are involved (cut-off distance equal to 2ℓ, i.e. $M=2$), with inter-atomic stiffnesses equal to k_1 and k_2 respectively.

2. In the other two cases, a periodic distribution of the bond stiffness coefficients along the atomic chain is assumed. In Case 3, $M=1$ as in Case 1, but the stiffness values are alternatively set to k_1^α and k_1^β. In Case 4, $M=2$ and the stiffness values are alternatively set to k_1^α and k_1^β for the nearest neighbor interactions, and to k_2^α and k_2^β for the next-nearest neighbor interactions. The unit cell has thus a length equal to 2ℓ. We note that Case 1 and Case 2 are special instances of Case 3 and Case 4, respectively.

Values of the equivalent Young's modulus obtained from the Cauchy–Born rule (Method 1) or from the notion of RVE (Method 2) are shown in Table I. We observe that both approaches give identical moduli in Cases 1 and 2. In the last two cases, Method 1 provides erroneous values as the structure fails to reach an equilibrium configuration under a homogeneous deformation. Although it is sometimes unclear how to rigorously define a RVE for more general materials, the continuum model will always be calibrated using the RVE approach in what follows. Two-dimensional and three-dimensional calibration examples can be found in [3, 13].

We now establish the weak formulation of the continuum problem in domain Ω. We assume that Dirichlet boundary conditions $\mathbf{u}=\mathbf{u}_D$ are prescribed on part $\partial\Omega^D$ of the boundary and that the structure is subjected to tractions $\mathbf{F}^c$ on $\partial\Omega^N$ and to a body force density $\mathbf{f}^c$ in Ω. We introduce the space of admissible solutions $\mathscr{V}_D=\{\mathbf{v}\in(H^1(\Omega))^d;\ \mathbf{v}=\mathbf{u}_D \text{ on } \partial\Omega^D\}$ and space of test functions $\mathscr{V}_0=\{\mathbf{v}\in(H^1(\Omega))^d;\ \mathbf{v}=\mathbf{0} \text{ on } \partial\Omega^D\}$. The formulation of the continuum problem, when ignoring the particle region, reads:

$$\boxed{\text{Find } \mathbf{u}\in\mathscr{V}_D \text{ such that } B^c(\mathbf{u};\mathbf{v})=F^c(\mathbf{v}) \quad \forall\mathbf{v}\in\mathscr{V}_0} \tag{12}$$

with

$$\begin{aligned} B^c(\mathbf{u};\mathbf{v}) &= \int_\Omega \mathbb{P}(\mathbf{u}):\frac{\partial\mathbb{F}}{\partial\mathbf{u}}(\mathbf{v})\,\mathrm{d}X \\ F^c(\mathbf{v}) &= \int_\Omega \mathbf{f}^c\cdot\mathbf{v}\,\mathrm{d}X+\int_{\partial\Omega^N}\mathbf{F}^c\cdot\mathbf{v}\,\mathrm{d}S \end{aligned} \tag{13}$$

and $\mathbb{P}=\partial\omega^c/\partial\mathbb{F}$ being the first Piola–Kirchhoff tensor.

DOI: 10.1002/nme

3. DESCRIPTION OF THE COUPLING METHOD

3.1. The Arlequin framework

The Arlequin method, which was originally developed as a general framework for coupling different models [8, 23], has been recently applied to the case of continuum and particle models in [3, 11]. We briefly recall the main features of the approach:

1. The computational domain Ω is first divided into two overlapping regions, i.e. a particle region Ω_a and a continuum region Ω_c. The overlap region is denoted by $\Omega_o = \Omega_a \cap \Omega_c$;
2. In Ω_o, energy contributions from the two models are added together by means of a partition of unity;
3. The continuum and discrete displacements are matched in Ω_o with respect to some measure defined below.

Let N_a be the number of particles in Ω_a, such that $N_a \ll N_p$, and let $\mathscr{W}_D = \mathbb{R}_D^{d\times N_a}$ and $\mathscr{W}_0 = \mathbb{R}_0^{d\times N_a}$ be the sets of trial and test functions, respectively. For the continuum model, we introduce the space of admissible solutions as $\mathscr{U}_D = \{\mathbf{v} \in (H^1(\Omega_c))^d;\ \mathbf{v} = \mathbf{u}_D \text{ on } \partial\Omega_c^D\}$ and space of test functions as $\mathscr{U}_0 = \{\mathbf{v} \in (H^1(\Omega_c))^d;\ \mathbf{v} = \mathbf{0} \text{ on } \partial\Omega_c^D\}$. The global potential energy of the coupled system reads:

$$W_p^{\mathrm{Arl}}(\mathbf{w}, \mathbf{u}) = \int_{\Omega_c} \alpha^c \omega^c(\mathbf{u})\,\mathrm{d}x - \int_{\Omega_c} \beta^c \mathbf{f}^c \cdot \mathbf{u}\ ,\mathrm{d}x - \int_{\partial\Omega_c^N} \beta^c \mathbf{F}^c \cdot \mathbf{u}\ ,\mathrm{d}S$$
$$+ \frac{1}{2}\sum_{i=1}^{N_a} \sum_{j\in\mathscr{N}_i} \alpha_{ij}^a V_{ij}(\mathbf{w}) - \sum_{i=1}^{N_a} \beta_i^a \mathbf{f}_i \cdot \mathbf{w}_i, \quad \forall (\mathbf{w}, \mathbf{u}) \in \mathscr{W}_D \times \mathscr{U}_D \tag{14}$$

Parameters $(\alpha_{ij}^a, \alpha^c)$ and (β_i^a, β^c) are weight coefficients that will be described below. In order to define the coupling operator, we introduce the space of Lagrange multipliers $\mathscr{M} = (H^1(\Omega_o))^d$ as well as the following operators:

1. The prolongation operator $\Pi : \mathscr{W}_D \longrightarrow \mathscr{M}$ which maps the discrete particle displacement into a continuous piecewise linear displacement on Ω_o;
2. The restriction operator $R : \mathscr{U}_D \longrightarrow \mathscr{M}$ which restricts the continuous displacement field to Ω_o;
3. The difference operator $D : \mathscr{W}_D \times \mathscr{U}_D \longrightarrow \mathscr{M}$ such that $D(\mathbf{w}, \mathbf{u}) = R\mathbf{u} - \Pi\mathbf{w}$.

We consider here a coupling operator based on the H^1-norm of the displacement such that

$$\|D(\mathbf{w}, \mathbf{u})\|_{\mathscr{M}}^2 = \int_{\Omega_o} [(D(\mathbf{w}, \mathbf{u}))^2 + \gamma(\nabla D(\mathbf{w}, \mathbf{u}))^2]\,\mathrm{d}X \tag{15}$$

where γ is a scaling factor, with corresponding inner product in $\mathscr{M}$:

$$C(\boldsymbol{\mu}, \lambda) = \int_{\Omega_o} [\boldsymbol{\mu} \cdot \lambda + \gamma \nabla \boldsymbol{\mu} : \nabla \lambda]\,\mathrm{d}X \tag{16}$$

The problem consists in searching the saddle-point of the Lagrangian:

$$\mathscr{L}(\mathbf{z}, \mathbf{v}, \boldsymbol{\mu}) = W_p^{\mathrm{Arl}}(\mathbf{z}, \mathbf{v}) - C(\boldsymbol{\mu}, D(\mathbf{z}, \mathbf{v})) \tag{17}$$

DOI: 10.1002/nme

It is recast as follows:

$$\boxed{\begin{array}{l}\text{Find } (\mathbf{w},\mathbf{u},\lambda)\in\mathscr{W}_D\times\mathscr{U}_D\times\mathscr{M} \text{ such that :}\\ \quad B^a_\alpha(\mathbf{w};\mathbf{z})+B^c_\alpha(\mathbf{u};\mathbf{v})-C(\lambda,D(\mathbf{z},\mathbf{v}))=F^a_\beta(\mathbf{z})+F^c_\beta(\mathbf{v}) \quad \forall(\mathbf{z},\mathbf{v})\in\mathscr{W}_0\times\mathscr{U}_0\\ \quad C(\boldsymbol{\mu},D(\mathbf{w},\mathbf{u}))=0 \quad \forall\boldsymbol{\mu}\in\mathscr{M}\end{array}} \tag{18}$$

where

$$\begin{aligned} B^a_\alpha(\mathbf{w};\mathbf{z}) &= \frac{1}{2}\sum_{k=1}^{N_a}\sum_{i=1}^{N_a}\sum_{j\in\mathscr{N}_i}\alpha^a_{ij}\frac{\partial V_{ij}(\mathbf{w})}{\partial\mathbf{z}_k}\cdot\mathbf{z}_k\\ F^a_\beta(\mathbf{z}) &= \sum_{i=1}^{N_a}\beta^a_i\mathbf{f}_i\cdot\mathbf{z}_i\\ B^c_\alpha(\mathbf{u};\mathbf{v}) &= \int_{\Omega_c}\alpha^c\frac{\partial\omega^c}{\partial\mathbb{F}}(\mathbf{u}):\frac{\partial\mathbb{F}}{\partial\mathbf{u}}(\mathbf{v})\,\mathrm{d}X\\ F^c_\beta(\mathbf{v}) &= \int_{\Omega_c}\beta^c\mathbf{f}^c\cdot\mathbf{v}\,\mathrm{d}X+\int_{\partial\Omega^N_c}\beta^c\mathbf{F}^c\cdot\mathbf{v}\,\mathrm{d}S \end{aligned} \tag{19}$$

Well-posedness of Problem (18) has been studied in [11, 15, 24] in the case of linear problems. The Arlequin problem can be solved using a finite element discretization of the continuum displacement and Lagrange multiplier fields. One of the key points of the Arlequin method is the choice of the approximation space for the Lagrange multiplier field. Studies reported in [11, 25] show that for the constraint operator given in (15), the mesh size used to discretize the Lagrange multipliers should be at least equal to the one used in the continuum region, and that it should be related to the RVE size considered to calibrate the continuum model.

3.2. Averaged partition of the energy

The weights (α^c,α^a_{ij}) and (β^c,β^a_i) enable to blend the energies of concurrent models in the overlap region Ω_o. Functions $\alpha^c(\mathbf{X})$ and $\beta^c(\mathbf{X})$ are required to satisfy:

$$\alpha^c(\mathbf{X})=\beta^c(\mathbf{X})=\begin{cases}1 & \forall\mathbf{X}\in\Omega_c\setminus\Omega_o\\ 0 & \forall\mathbf{X}\in\Omega_a\setminus\Omega_o\end{cases} \tag{20}$$

In Ω_o, $\alpha^c(\mathbf{X})$ and $\beta^c(\mathbf{X})$ may be chosen constant, piecewise constant, linear, cubic, or as higher-order polynomial functions. Generally, we take $\alpha^c=\beta^c$. We then derive $(\alpha^a_{ij},\beta^a_i)$ with the formula

$$\begin{aligned}\alpha^a_{ij} &= 1-\frac{1}{|S_{ij}|}\int_{S_{ij}}\alpha^c(\mathbf{X})\,\mathrm{d}x\\ \beta^a_i &= 1-\beta^c(\mathbf{x}_i)\end{aligned} \tag{21}$$

so that the weights for the particle and continuum models define a partition of unity (in an average sense). S_{ij} denotes the physical region of influence of the bond between particle i and particle j. In the 1D case, S_{ij} merely corresponds to the bond support itself, and $|S_{ij}|=|x_j-x_i|$. In 2D and

DOI: 10.1002/nme

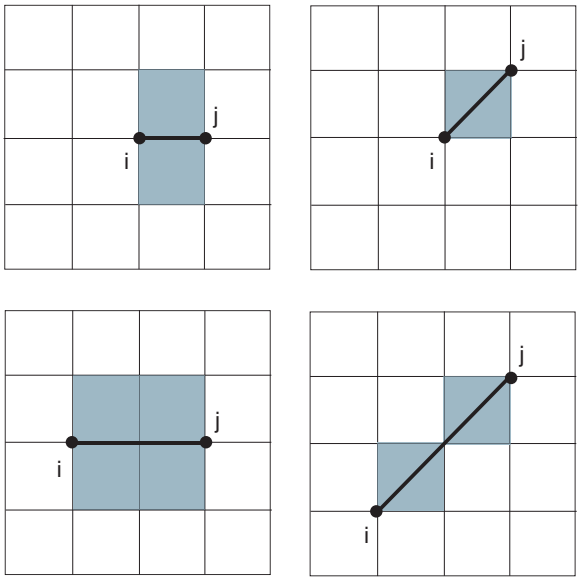

Figure 3. Examples of regions S_{ij} used to compute the weight coefficients α^a_{ij} between particle i and particle j. The bond is represented by a thick segment while the region S_{ij} is the domain colored in light grey. The top row of figures shows cases of nearest neighbor interactions, while the bottom row considers next-nearest neighbor interactions.

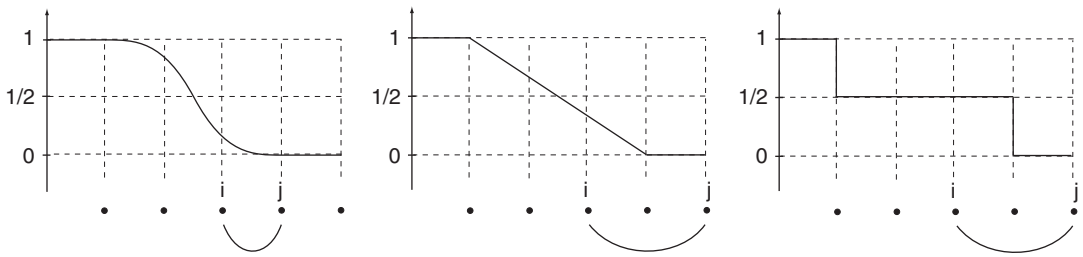

Figure 4. Three examples of weight function α^c: cubic function (left), piecewise linear function (center), and piecewise constant function (right).

3D cases, S_{ij} corresponds to the region adjacent to the bond between particle i and particle j, as illustrated in Figure 3.

The definition of α^a_{ij} through an average is a consistent way to weigh particle energy, implicitly defining an energy density at the particle scale. This is an extension of the choice made in the previous work [11], i.e. $\alpha^a_{ij} = 1 - \alpha^c((\mathbf{x}_i + \mathbf{x}_j)/2)$. Differences between these approaches are observed when considering high-order polynomial weights, or long–range interactions, as illustrated in the three 1D examples of Figure 4. The first case considers a cubic polynomial function $\alpha^c(x)$ in the overlap region Ω_o, and deals with the weighting term α^a_{ij} associated with a bond between

DOI: 10.1002/nme

nearest neighbors. It is easy to show that in that case:

$$\alpha_{ij}^a = 1 - \frac{1}{|S_{ij}|}\int_{x_i}^{x_j} \alpha^c(x)\,\mathrm{d}x \neq 1 - \alpha^c\left(\frac{x_i + x_j}{2}\right) \tag{22}$$

In the second case, we consider a linear function $\alpha^c(x)$ in Ω_o and deal with a bond between next-nearest neighbors, which overlaps the discontinuity. We have in that case $1-\alpha^c((x_i+x_j)/2)=1$ whereas the value α_{ij}^a computed with the integral is less than one and is consistent with the coupling. In the third case, we deal with the same bond as in case 2, but consider a piecewise constant function $\alpha^c(x)$ (discontinuous at the midpoint of the bond). In that case, the value of α^c at midpoint is not defined but the definition of α_{ij}^a as an average remains valid and leads naturally to the value $\alpha_{ij}^a = 0.75$.

4. ANALYSIS OF SPURIOUS EFFECTS IN THE ARLEQUIN FORMULATION

Because the Arlequin problem is based on a global energy formulation, it creates ghost forces along the overlap region, as in the quasi-continuum method [9], when the interaction potentials involve next-nearest neighbors. The notion of ghost force was introduced for the quasi-continuum method in [17] and analyzed in several works thereafter (a general overview can be found in [20]). Ghost forces are non-physical forces that arise in coupling models based on the minimization of a global energy, i.e. on a minimization of a functional biased with non-symmetric interactions due to the presence of local and non-local particles. Even in the case where only nearest neighbors are considered, other spurious effects may arise in the Arlequin framework depending on the definition of the coupling operator and discretization scheme. For example, it was shown earlier [11, 15, 25] that the finite element space for the Lagrange multipliers had to be carefully chosen to avoid non-physical effects (locking, etc.). In particular, it has been established that the associated element size had to be at least larger than the representative cell used to define the continuum problem (RVE) and could not be smaller than the size of the finite elements in the continuum region (assuming that the representative particle scale is smaller). In the following, we ensure that the Lagrange multiplier is discretized on a finite element mesh that coincides with the mesh used in the continuum region while selecting a mesh size equal to a multiple of the RVE size. However, under these conditions, we may still observe spurious effects [11]. We now review these effects on the one-dimensional model problem described in Figure 5. We will propose corrective methods in the next section.

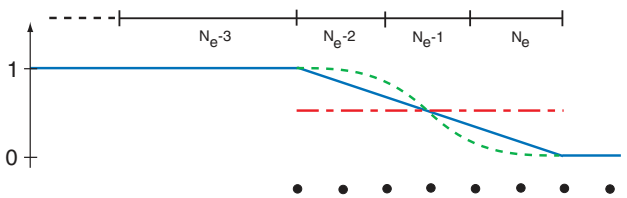

Figure 5. The 1D Arlequin method with constant (dash-dotted line), linear (solid line), and cubic (dash line) weight functions.

DOI: 10.1002/nme

Assuming that only the particle region Ω_a is subjected to loading and using linear elasticity for the continuum model, the continuous 1D formulation of the Arlequin problem (18) reads:

$$\begin{aligned}&\text{Find } (u, \mathbf{w}, \lambda) \in \mathscr{U}_D \times \mathscr{W}_D \times \mathscr{M} \text{ such that:}\\ &\int_{\Omega_c} \alpha^c(x) E^{\mathrm{eq}} \frac{\mathrm{d}u}{\mathrm{d}x}\frac{\mathrm{d}v}{\mathrm{d}x}\,\mathrm{d}x + \frac{1}{2}\sum_{i=1}^{N_a}\sum_{j\in\mathscr{N}_i} \alpha^a_{ij} k_{ij}(w_j - w_i)(z_j - z_i)\\ &\qquad -C(\lambda, D(\mathbf{z}, v)) = \sum_{i=1}^{N_a} f_i z_i \quad \forall (\mathbf{z}, v) \in \mathscr{W}_0 \times \mathscr{U}_0\\ &\qquad -C(\mu, D(\mathbf{w}, u)) = 0 \quad \forall \mu \in \mathscr{M}\end{aligned} \tag{23}$$

We introduce the finite element spaces $\mathscr{U}^h_0 \subset \mathscr{U}_0$ and $\mathscr{M}^h \subset \mathscr{M}$ of continuous piecewise linear functions for the continuum solution and the Lagrange multiplier, respectively. The discrete version of (23) then reads:

$$\begin{aligned}&\text{Find } (u_h, \mathbf{w}_h, \lambda_h) \in \mathscr{U}^h_D \times \mathscr{W}_D \times \mathscr{M}^h \text{ such that:}\\ &\sum_{e=1}^{N_e} \alpha^c_e \frac{E^{\mathrm{eq}}}{h_e}(u^e_{h,1} - u^e_{h,2})(v^e_{h,1} - v^e_{h,2}) + \frac{1}{2}\sum_{i=1}^{N_a}\sum_{j\in\mathscr{N}_i} \alpha^a_{ij} k_{ij}(w_{h,j} - w_{h,i})(z_{h,j} - z_{h,i})\\ &\qquad -C(\lambda_h, D(\mathbf{z}_h, v_h)) = \sum_{i=1}^{N_a} f_i z_i \quad \forall (\mathbf{z}_h, v_h) \in \mathscr{W}_0 \times \mathscr{U}^h_0\\ &\qquad -C(\mu_h, D(\mathbf{w}_h, u_h)) = 0 \quad \forall \mu_h \in \mathscr{M}^h\end{aligned} \tag{24}$$

where $\alpha^c_e = \int_e \alpha^c(x)\,\mathrm{d}x$ is the weight associated with the continuum energy in element e, E^{eq} is the Young's modulus derived from homogenization, h_e is the element size, N_e is the number of elements in Ω_c, and $u^e_{h,1}$ and $u^e_{h,2}$ are the degrees of freedom associated with the nodes of element e. The weight function α^c and α^a in the overlap region Ω_o will be alternatively chosen as the constant, linear, or cubic functions such as those shown in Figure 5. We will denote by s the number of nearest neighbor bonds lying in each element. The parameter s takes the same value in all elements as we shall consider uniform meshes only. We also recall that ℓ refers to the distance separating two consecutive particles in the reference configuration of the one-dimensional chain.

We first consider the ideal case where only nearest-neighbor interactions with homogeneous bond coefficients $k_{ij} = k = 100$ are involved ($M = 1$). The chain of particles is fixed at $x = 0$ and subjected to a traction force $F = E^{\mathrm{eq}}/L$ at $x = L = 8$. We take $\Omega_c = (0, 4.8)$, $\Omega_a = (3.2, 8)$, and $\Omega_o = \Omega_a \cap \Omega_c = (3.2, 4.8)$. Furthermore, we set $\ell = 0.2$ and $s = 1$. As expected, the displacement at L is equal to unity for the three types of weight function and the strain field is constant (see left plot of Figure 6). Only the Lagrange multipliers vary whether we choose α^c constant, linear, or cubic (see right plot of Figure 6).

4.1. Free modes

In order to illustrate the presence of free modes, we use the same example as above in the case where α^c is constant or linear. We however select here $s = 4$. We observe in Figure 7 that the

DOI: 10.1002/nme

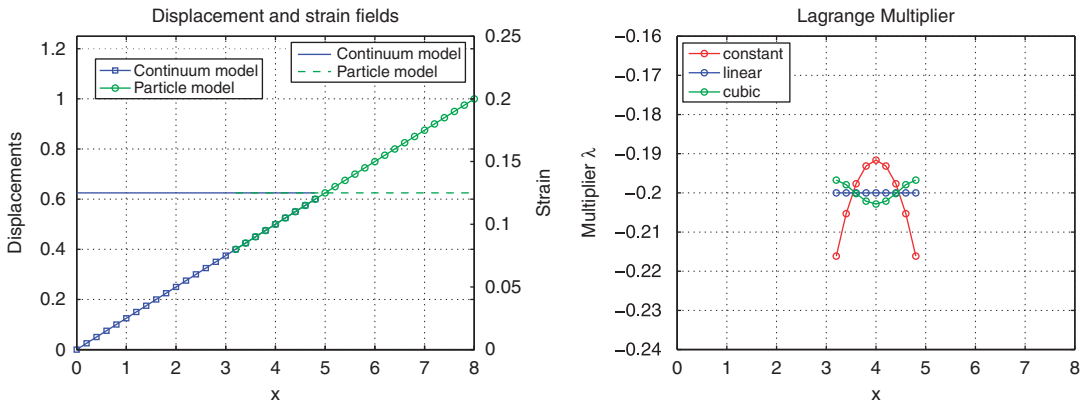

Figure 6. Displacement and strain fields (left) and Lagrange multiplier field with respect to the weight function (right).

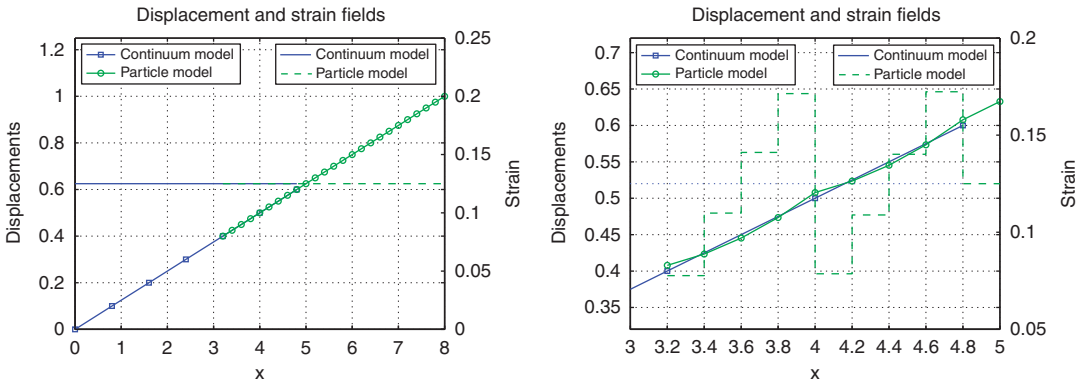

Figure 7. Displacement and strain fields obtained with a linear (left) or a constant (right) weight function α^c. Displacement and strain fields for a constant weight function have been zoomed in the overlap region.

displacement at L is 1.0078 for α^c constant and exactly 1.00 for α^c linear. This is due to the fact that the particle solution oscillates around the continuum displacement in the overlap region when α^c is constant. Such a phenomenon is not seen for α^c linear nor for a cubic weight function. These modes did not arise in the previous example as the particle solution was locked to the continuum solution through the Lagrange multipliers.

4.2. Local loss of coercivity

We repeat the previous experiments with $s=2$, 4, and 8 in the case α^c is cubic (see Figure 8). We observe that the continuum and particle solutions deteriorate as s increases. This is due to the fact that the problem becomes locally ill-posed as the energy of the particles is weighted by a coefficient that tends to zero in the left most bond of the overlap region. In general, local loss of coercivity is noticeable when the mesh size and bond size are very different and when the weight

DOI: 10.1002/nme

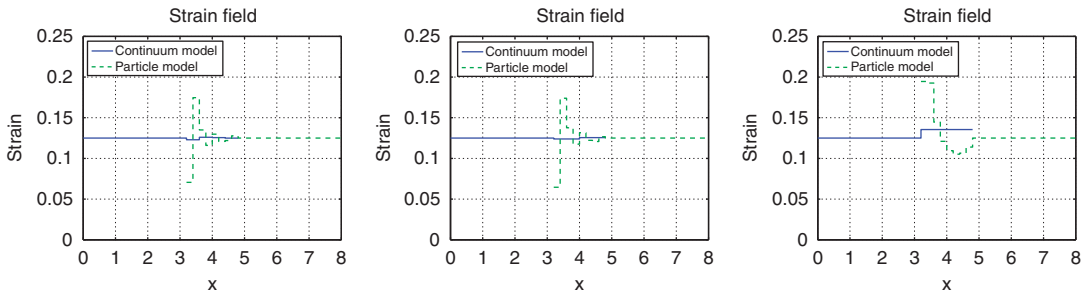

Figure 8. Strain field obtained with a cubic weight function, in the cases $s=2$ (left), $s=4$ (center), and $s=8$ (right).

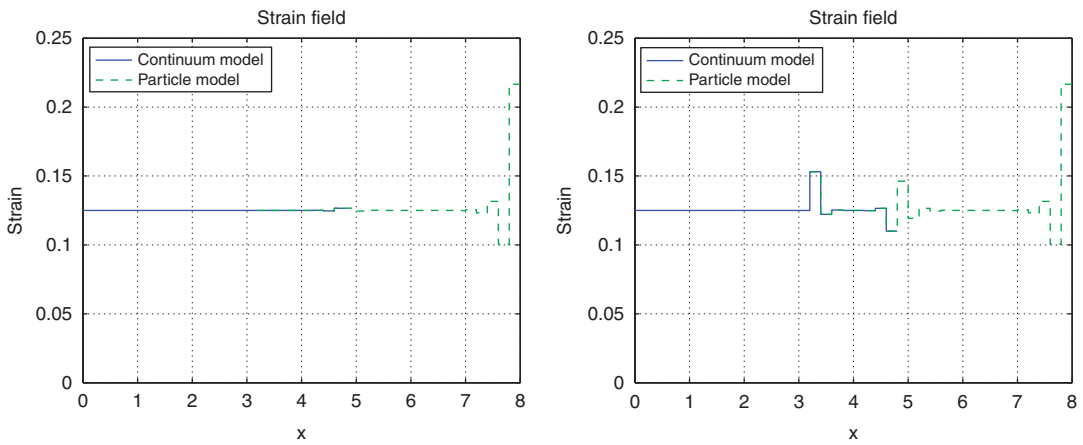

Figure 9. Strain field obtained with $h=1$, for linear (left) and constant (right) weight functions.

function 'quickly' tends to zero in part of the overlap region. This effect does not arise for instance with linear weights for $s=2$, 4, or 8. This effect was previously analyzed in [15] in the case when two continuum models are coupled together.

4.3. Spurious effects in the case of long-range interactions

Ghost forces arise in the Arlequin approach whenever the particle model involves long–range interactions, as in the quasi-continuum method [26]. These ghost forces are created from truncating the particle domain in the overlap region, which incurs a loss of symmetry in the formulation of the problem. For example, we show in Figure 9 the strain fields obtained with $s=1$ but considering nearest and next-nearest neighbor interactions ($M=2$) with spring constants $k_1=100$ and $k_2=50$, respectively. We recall that the continuum and particle displacements are locked together on the overlap region Ω_o as the finite element mesh for the Lagrange multiplier exactly coincides with

DOI: 10.1002/nme

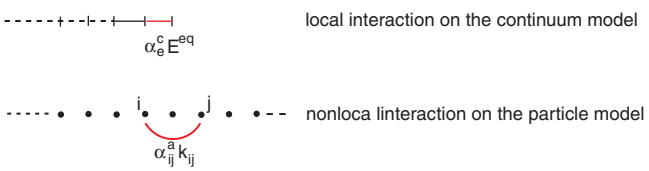

Figure 10. An example of interaction creating 'ghost force' type effects in the Arlequin framework. The energy of the interaction between particles i and j is split into a local contribution with weight α_e^c and a nonlocal contribution with weight α_{ij}^a.

the fine scale lattice as $s=1$. We observe that the presence of long–range interactions induces distinctive phenomena at the two extremities of the overlap region:

1. Left side of Ω_o: here the particles near the boundary of the atomic region Ω_a do not 'see' the neighboring particles that they would normally interact with if the full particle system were considered. This induces surface perturbations due to the non-locality of the particle model. Note that such a behavior is also observed for the same reason at the boundary $x=L$. We nevertheless observe that these effects attenuate as the weights associated with the missing bonds become small, which is the case when linear and cubic weights are used (see Figure 9).
2. Right side of Ω_o: effects which occur near the right side of Ω_o can be attributed to ghost forces as revealed in the case of the quasi-continuum method. They are due to the fact that the energy contribution from the continuum model is local while that from the particle model is essentially non-local. Therefore, the energy of the closest bonds to the interface between Ω_o and $\Omega_a \backslash \Omega_o$ (see Figure 10) is a combination of a non-local energy, weighted by α_{ij}^a, and a local energy, weighted by α_e^c, which creates unsymmetric contributions between the two interacting particles of each bond. The distribution of energy is therefore non-symmetric, which locally affects the global stiffness matrix and leads to spurious effects.

As a result of these experiments, it is clear that linear or cubic weight functions are better suited than constant functions to control some of the spurious effects (particularly free modes and long–range interaction effects). However, the use of such weight functions is not sufficient to cancel all spurious effects. We propose to develop some corrective methods in the next section in order to remedy this issue.

5. CORRECTIVE TECHNIQUES FOR THE ARLEQUIN COUPLING METHOD

5.1. Formulation with phantom particles

In order to avoid surface effects, an idea is to add phantom particles in the continuum subregion Ω_c/Ω_o and close to the interface. The role of these particles is similar to the one played by the so-called pad atoms in the quasi-continuum method [17, 20] and in the standard bridging-domain method [27]. In doing so, we modify the total energy of the system, but the perturbation can be kept minimal if these particles are assigned a very small energy by means of an infinitely small weight coefficient $\varepsilon > 0$. We consider two possible approaches for the definition of the modified weight functions α^c and α^a due to these extra particles, as shown in Figure 11. On the left sketch,

DOI: 10.1002/nme

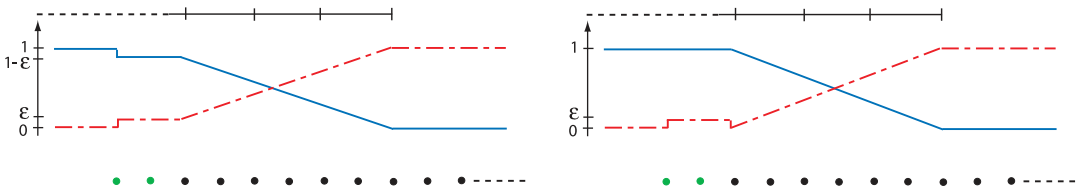

Figure 11. Extra particles added to the Arlequin formulation and corresponding weight functions: α^c (solid line) and α^a (dash-dotted line).

we show the case where the coefficient α^a is defined as $\alpha^a(x) = 1 - \alpha^c(x)$, $\forall x \in \Omega$, so that the global energy is rigorously conserved. On the right sketch, we consider the case where the energy of the phantom particles is simply added to the global energy, which obviously yields a non-conservative method. However, for very small ε, the latter is almost consistent and we use, for practical reasons, the second approach in the numerical examples presented below.

We now consider an example in which $s = 1$, α^c is constant, and interactions between particles involve nearest and next-nearest neighbors. We compare the strain and Lagrange multiplier computed with or without inserting two phantom particles. The value of ε is set to 10^{-5}. The results are shown in Figure 12. We observe that the method somewhat attenuates the surface effects on the left of Ω_o. We actually show below that the addition of phantom particles proves to be essential for the corrective technique that we propose. We expect that these phantom particles help provide an accurate approximation of the location of the particles in Ω_c/Ω_o without resorting to the Cauchy–Born rule. However, this fact is not guaranteed; indeed, replacing $s = 1$ by $s = 2$ in the previous example, we observe that the strain exhibits large oscillations around the phantom particles that propagate far into the particle region (see Figure 13). Another situation for which we may fail to predict the correct position of the phantom particles is the case of heterogeneous lattices. In order to get a better approximation of the physical position of the phantom particles, we prefer to resort to a method in which the strain field of the phantom particles is duplicated from the nearest RVE as shown in Figure 14.

Remark 1

The method may lead to positions of phantom particles that do not coincide with the actual ones. Nevertheless, a reasonable approximation of these positions is sufficient as they have a limited impact in the proposed correction method.

5.2. *Computation of dead forces*

Using the discrete Arlequin Equations (24), we can compute the resulting forces at each node of the finite element mesh and at each particle of the discrete system. Indeed, given the displacements $(u_h, \mathbf{w}_h)$,

1. The resulting force F_k^c acting at a given node k in the continuum region Ω_c is:

$$F_k^c = \sum_{i=1}^{2} \alpha_{e_i}^c \frac{E^{\mathrm{eq}}}{h_{e_i}} (u_{h,i}^{e_i} - u_h^k) + \frac{\partial C(\mu_h, D(\mathbf{w}_h, u_h))}{\partial u_h^k} \tag{25}$$

DOI: 10.1002/nme

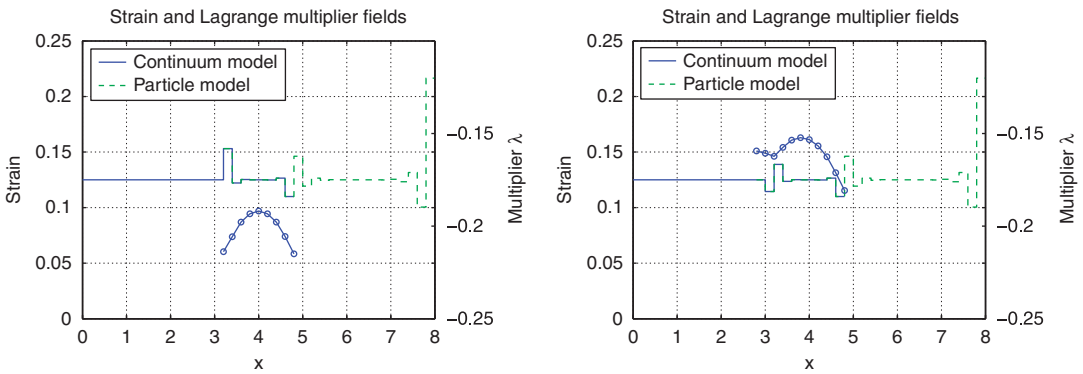

Figure 12. Influence of phantom particles on the strain and Lagrange multiplier fields: without (left) and with (left) extra particles.

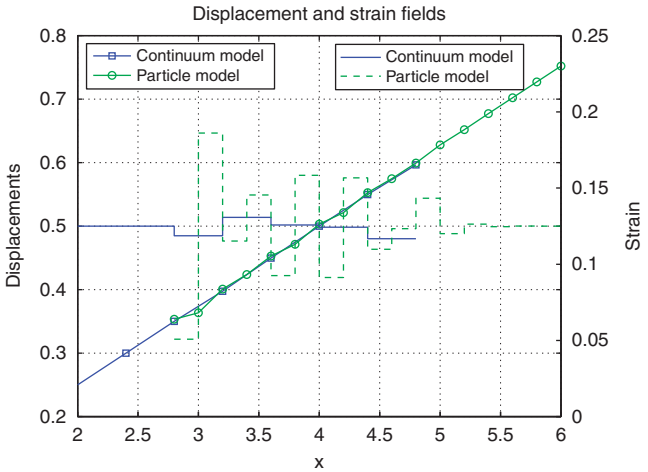

Figure 13. Displacement and strain fields with phantom particles for $s=2$.

where e_1 and e_2 provide the indices of the left and right elements connected to node k and u_h^k is the nodal displacement of node k;

2. The resulting force F_i^a acting at a particle i in Ω_a is:

$$F_i^a = \sum_{j \in \mathcal{N}_i} \alpha_{ij}^a k_{ij}(w_j - w_i) + \frac{\partial C(\mu_h, D(\mathbf{w}_h, u_h))}{\partial w_i} + \beta_i^a f_i \tag{26}$$

When solving the coupled problem (notice that the problem is linear in 1D, but nonlinear in 2D and 3D due to geometric nonlinearities, in which case we use the steepest-descent or Newton method), particles and nodes are at equilibrium, so that $F_k^c = 0$, $\forall k$, and $F_i^a = 0$, $\forall i$. Using the approach developed for the quasi-continuum [17, 20], we can introduce the so-called dead forces representing the difference between the actual forces acting at the nodes and particles and the forces calculated as if the nodes or particles were in a fully continuum or particle region.

DOI: 10.1002/nme

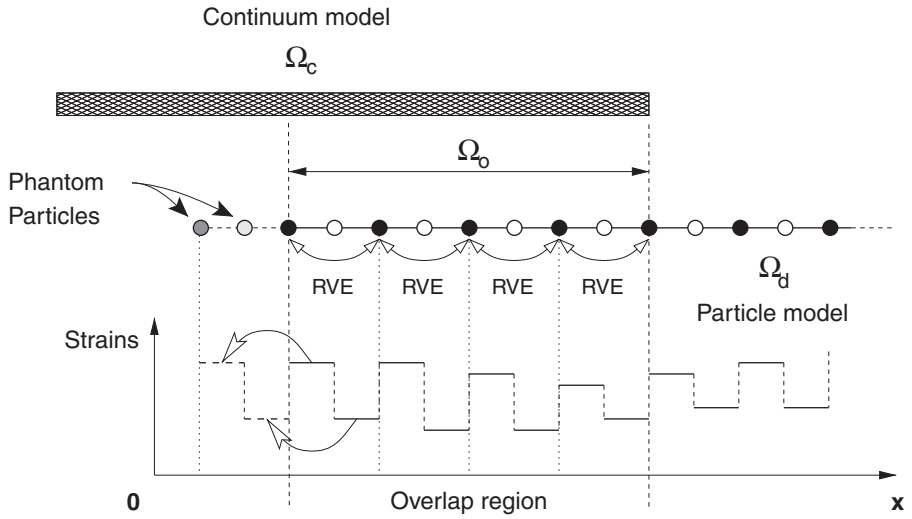

Figure 14. Duplication of the strain field of the last RVE to get the position of the phantom particles.

We denote by g_k^c and g_i^a the corresponding dead forces for node k and particle i, respectively. They read:

$$\begin{aligned} g_k^c &= -\sum_{i=1}^{2} \frac{E^{\text{eq}}}{h_{e_i}} (u_{h,i}^{e_i} - u_h^k) \\ g_i^a &= -\sum_{j \in \mathcal{N}_i} k_{ij}(w_j - w_i) - f_i \end{aligned} \tag{27}$$

We emphasize that we do not make use of the Cauchy–Born rule here to compute the dead forces since phantom particles are explicitly introduced in the formulation. For these phantom particles, the corresponding dead forces may be incorrectly computed as they do not interact with all their actual neighbors. We will see however that the dead forces associated with phantom particles are irrelevant anyway.

5.3. Formulation involving dead forces

From (25) and (26), we see that internal forces are partitioned between the two concurrent models in the overlap region. Respecting the philosophy of the Arlequin approach, we introduce the dead forces (27) in a consistent manner in terms of the partition of unity, i.e. with respect to the weight functions α^c and α^a. The Lagrangian at the discrete level is then modified such that (in 1D):

$$\widehat{\mathscr{L}}(\mathbf{z}_h, v_h, \mu_h) = \widehat{W}_p^{\text{Arl}}(\mathbf{z}_h, v_h) - C(\mu_h, D(\mathbf{z}_h, v_h)) \tag{28}$$

where $\widehat{W}_p^{\text{Arl}}$ is the new potential energy of the coupled system defined by:

$$\widehat{W}_p^{\text{Arl}}(\mathbf{z}_h, v_h) = W_p^{\text{Arl}}(\mathbf{z}_h, v_h) - \sum_k \alpha^c(\mathbf{X}_k) g_k^c v_h^k - \sum_i \alpha^a(\mathbf{x}_i) g_i^a z_i \tag{29}$$

DOI: 10.1002/nme

1. Prescribe a value of the stopping criterion γ_{stop}.
2. Solve the corrected Arlequin problem by minimizing the potential energy (29). Dead forces are initialized to zero at the first iteration.
3. Duplicate the strain field of the last RVEs to get the position of phantom particles.
4. Compute the dead forces g_k^c (for each node k of the finite element mesh) and g_i^a (for each particle i of the discrete system).
5. Apply the weight coefficients α^c or α^a to the dead forces to get weighted dead forces $\alpha^c(\mathbf{X}_k)g_k^c$ and $\alpha^a(\mathbf{x}_i)g_i^a$.
6. Compute the maximal value
$$g_{max} = \max_{k,i}(|\alpha^c(\mathbf{X}_k)g_k^c|, |\alpha^a(\mathbf{x}_i)g_i^a|)$$
then normalize g_{max} as $\bar{g}_{max} = g_{max}/g_0$, where the normalization term g_0 is the value of a characteristic force in the problem (for our 1D example, g_0 corresponds to the traction force in the chain).
7. If $\bar{g}_{max} \leq \gamma_{\text{stop}}$, then stop. Otherwise, go to step 2.

Figure 15. Algorithm for the iterative correction method with dead forces.

where W_p^{Arl} is the potential energy in 1D corresponding to the one defined in (14). The corrective procedure is applied in an iterative manner to account for relaxation and an outline of the algorithm is shown in Figure 15. The potential energy at iteration $n+1$ involves the dead forces computed from nodal and particle displacements at iteration n. We will see in the numerical experiments below that the proposed corrective method allows to reach the correct solution of the problem as long as the concurrent models are compatible and the choice of the finite element space for the Lagrange multipliers guarantees that the exact solution does exist. However, we have not studied the convergence of the method from a theoretical viewpoint, namely, we do not know whether convergence of the corrective method is guaranteed. This will be the subject of future research work. Nevertheless, a few remarks are in order:

Remark 2
We emphasize that the dead forces are calculated everywhere in domain Ω, and not only in the overlap region, and that they are all included in the corrective formulation (29).

Remark 3
When the weight function α^c is discontinuous at the location of a node or a particle, weights for the dead forces may not be conveniently defined. Several limit values may be used, which should not affect the results.

Remark 4
We clearly see here that, although dead forces for phantom particles may be incorrectly evaluated, due to missing particles, they are weighted by a very small coefficient and are thus negligible. It is also interesting to notice that phantom particles are not necessary in some special cases, for instance when nearest neighbors with linear weights are considered or when the Cauchy–Born rule applies. In the former case, the dead forces involving the displacement of phantom particles are multiplied by zero; in the latter case, the position of the phantom particles is implicitly deduced from interpolation of the continuum displacement field and surface effects are straightforwardly corrected by the dead forces.

DOI: 10.1002/nme

Remark 5
It is also possible to use ideas similar to QC-GFC (Ghost-Forces Corrected) (see e.g. [19, 20]) with a domain decomposition. The problem is split into a continuum problem with energy (in the 1D case):

$$\frac{1}{2}\sum_{e=1}^{N_e}\frac{E^{\mathrm{eq}}}{l_e}(u^h_{e,2}-u^h_{e,1})^2$$

and a particle problem with energy:

$$\frac{1}{4}\sum_{i=1}^{N_a}\sum_{j\in\mathcal{N}_i}k_{ij}(z_j-z_i)^2$$

The two problems are solved iteratively and are constrained to each other. However, the method tends to converge very slowly, and for that reason, will not be investigated in this paper.

6. NUMERICAL RESULTS

In this section, we apply the corrective method to one-dimensional and two-dimensional problems to demonstrate the performance of the method. In the examples shown below, we always assume that the coupling region Ω_o is constructed in such a way that particles and boundaries of finite elements lie on the boundary of Ω_o.

6.1. One-dimensional examples with homogeneous bond stiffness

We consider here a homogeneous lattice; phantom particles are thus not required to obtain the dead forces. We first analyze cases where only nearest neighbors are taken into account and then consider cases with nearest and next-nearest neighbors. We demonstrate the efficiency of the corrective method on the test examples of Section 4 using the same numerical setting and modeling options.

1. *Correction of free modes*: We correct here the effects described in Section 4.1. We show in Figure 16 the dead forces at each iteration (weighted by α^c and α^a, chosen constant in this experiment) and the resulting corrected strain field.
2. *Correction of loss of coercivity*: We now show how the spurious effects due to the loss of coercivity observed in Section 4.2 can be corrected (recall that the weight coefficients are chosen cubic here). The weighted dead forces at each iteration and the resulting corrected strain field are displayed in Figure 17 and should be compared to the results of Figure 8 in the case where $s=4$.
3. *Correction of effects due to long–range interactions*: Effects due to long–range interactions are those described in Section 4.3. We choose here a constant weight α^c. Two configurations are considered: (i) in the first case, no phantom particles are introduced. In this case, the initial Arlequin solution is the one shown on the left plot of Figure 12. Dead forces are then used to correct the surface effects and ghost forces. Dead forces on the left side of Ω_a are computed by employing the Cauchy–Born rule; (ii) in the second case, phantom particles are considered and the initial Arlequin solution is shown on the right plot of Figure 12. Only the ghost forces need to be attenuated. Here we use the displacement of phantom particles to

DOI: 10.1002/nme

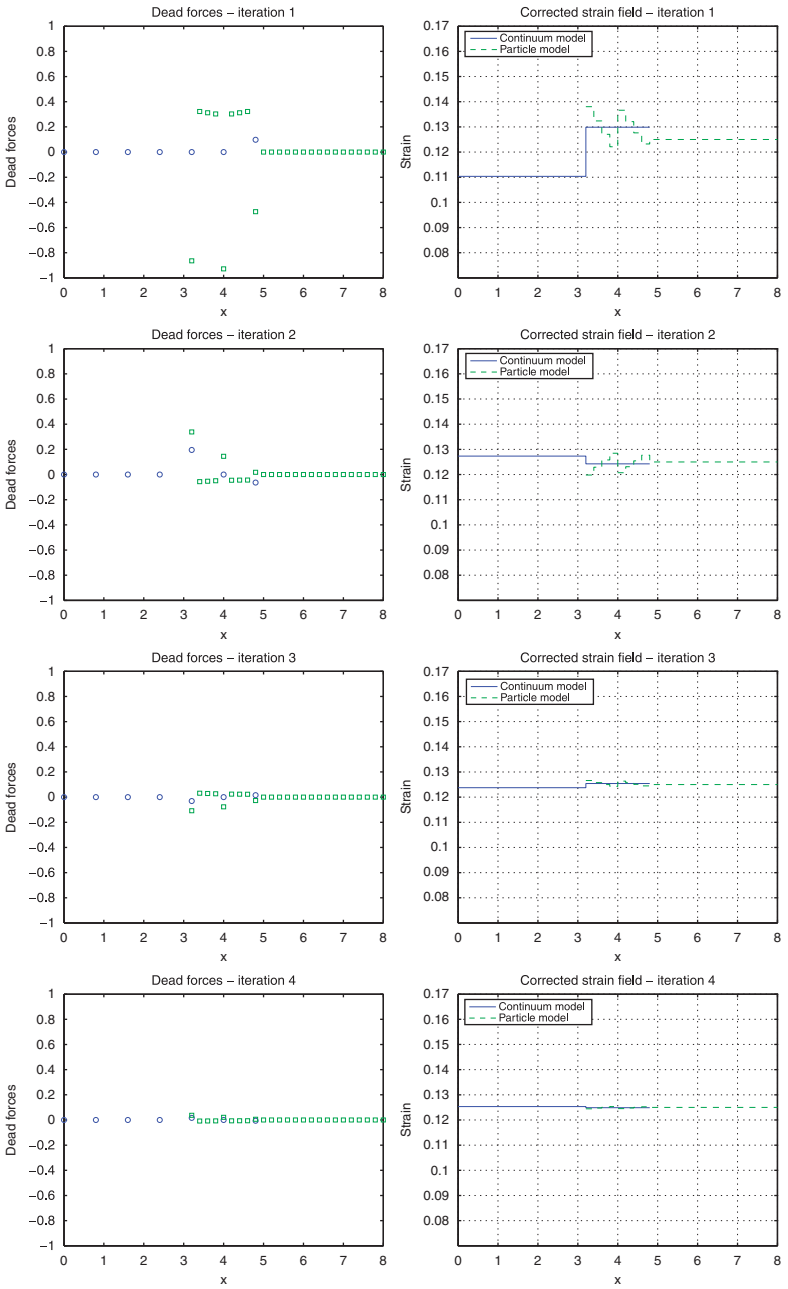

Figure 16. Weighted dead forces (left) and strain field (right) obtained at each iteration of the correction method.

DOI: 10.1002/nme

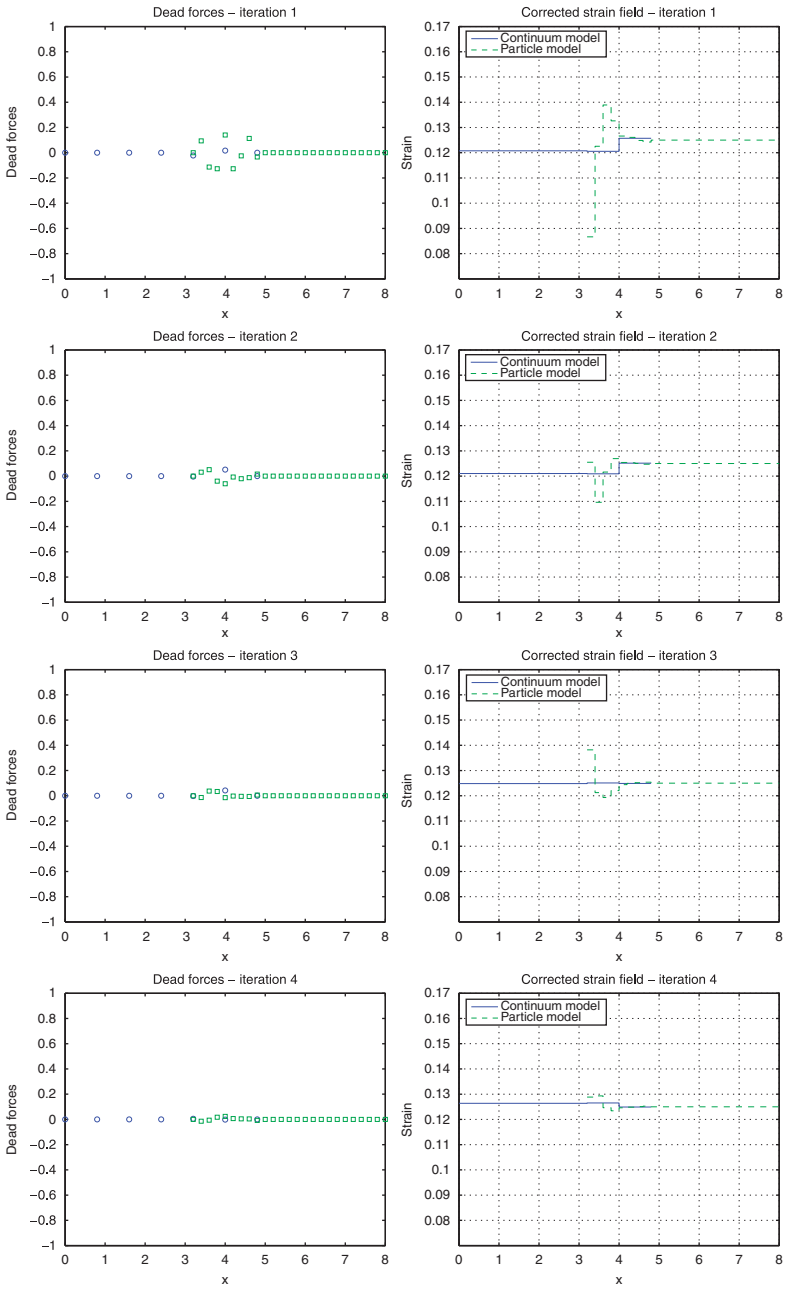

Figure 17. Weighted dead forces (left) and strain field (right) obtained at each iteration of the correction method.

DOI: 10.1002/nme

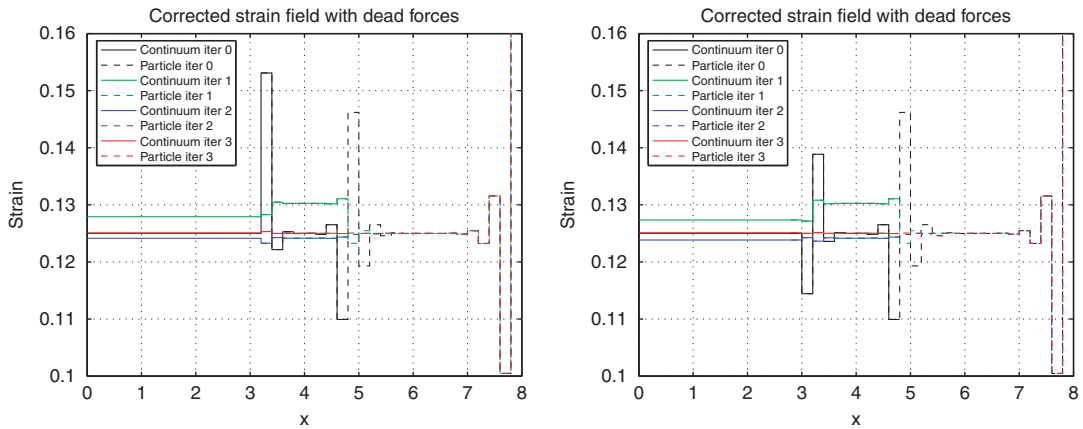

Figure 18. Strain field obtained at each iteration of the correction method, for a configuration without (left) or with (right) phantom particles.

compute the dead forces. Finally, we show in Figure 18 the corrected strain fields obtained, for both cases, after the first three iterations.

6.2. *One-dimensional examples with heterogeneous bond stiffness*

In this section, we apply the method to the case of heterogeneous bond coefficients. We set the RVE length to 2ℓ and we use $s=2$ to get a consistent coupling when discretizing the Lagrange multiplier field on the continuum mesh.

1. *Nearest neighbors only*: We first consider a chain of particles connected by periodically distributed covalent bonds with stiffness coefficients $k_1=100$ and $k_2=70$. No spurious effects are noticed using a linear weight function α^c, but they appear (due to the truncation of the particle lattice) when using a constant weight function α^c (see Figure 19). In the latter case, the spurious effects are attenuated by including dead forces to the formulation. These dead forces are computed by adding two phantom particles whose positions are constrained to be equal to those of the particles lying in the neighboring representative volume element. We obtain the corrected strain fields shown in Figure 20.
2. *Nearest and next-nearest neighbors*: We take $k_1=100$, $k_2=70$, and $k_3=k_4=50$, and we use constant or cubic weight function α^c. In the case of the constant weight function, the spurious effects are corrected with the same method as the one used in the previous example. In the case of a cubic weight function, we do not resort to phantom particles. The results displayed in Figure 21 clearly show that phantom particles are not necessary since the weighted dead forces are negligible. Again, we point out that the behavior observed on the right end of the structure is due to the combined effect of next-nearest neighbor interactions and truncation of the lattice. We do not modify the formulation there as it pertains to the modeling of the boundary condition. Finally, we show in Figure 22 a case where the coupling is overconstrained, so that the corrective method fails to converge to the correct solution. We choose $s=1$, i.e. the Lagrange multiplier field is discretized such that we enforce locking in Ω_o between the displacements of the continuum and particle models. Such a constraint is clearly incompatible with the heterogeneous nature of the molecular model.

DOI: 10.1002/nme

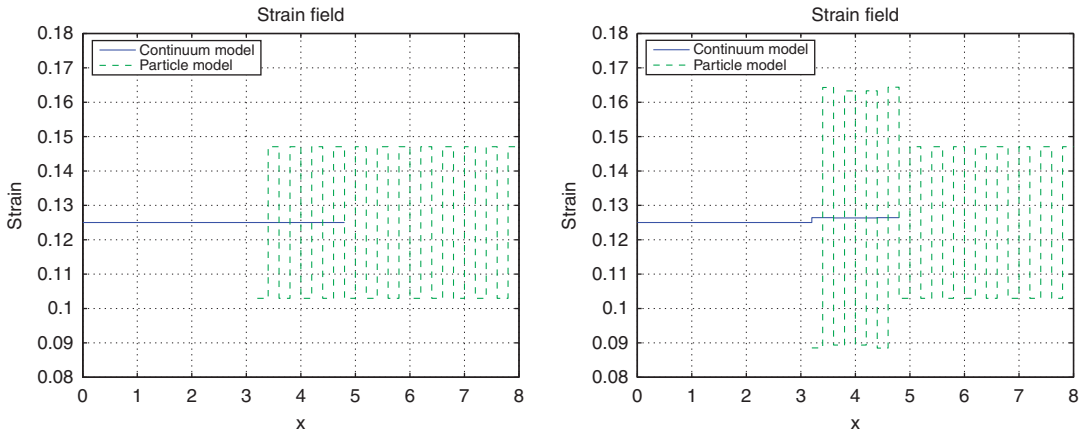

Figure 19. Strain field with heterogeneous bonds when using linear (left) or constant (right) weight function α^c.

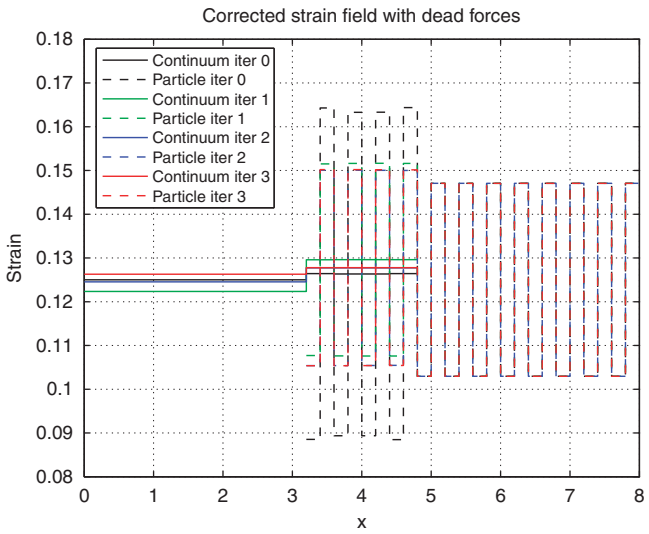

Figure 20. Corrected strain field at each iteration with heterogeneous bonds and constant weight function α^c.

6.3. Two-dimensional example

In this example, we consider a regular squared lattice Ω constituted of 51×51 particles with characteristic length $\ell = 0.1$, as shown in Figure 23. Particles on the boundary $\partial\Omega$ are fixed, and a pointwise force $\mathbf{F}$ is applied to the particle at the center. This induces a localized region Ω_a with large deformations in which the particle model should be used as the linear elasticity model is predicted to fail; in the remainder of Ω, we replace the lattice by an equivalent continuum model. Particles are supposed to interact with first, second, and third range neighbors (see Figure 24). We consider homogeneous

DOI: 10.1002/nme

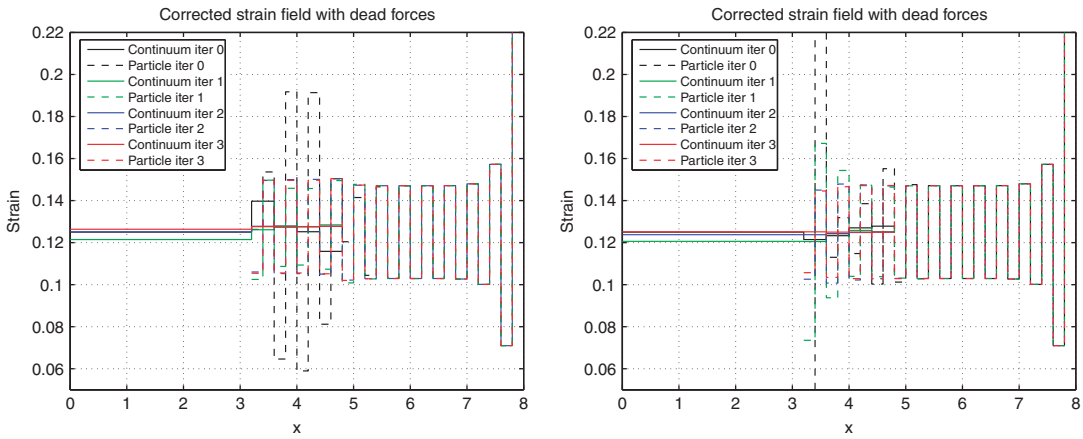

Figure 21. Corrected strain fields at each iteration with a constant (left) or a cubic (right) weight function α^c.

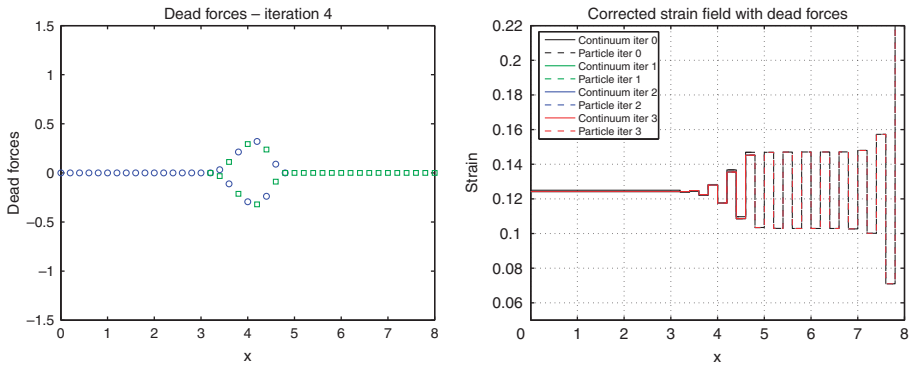

Figure 22. Weighted dead forces (left) and corrected strain field (right) computed at each iteration. The solution does not converge to the exact solution due to overconstraints.

stiffness coefficients $k_1 = 10$, $k_2 = 5$, and $k_3 = 10$. The large value of k_3 enables to study the effects of long–range interactions.

The linear elasticity model assumes cubical symmetry and a plane stress state. The values of the material parameters (E, G, ν) are thus calibrated with respect to the constitutive relation (in the (x, y) coordinate system associated with cubical symmetry):

$$\begin{pmatrix} \varepsilon_{xx} \\ \varepsilon_{yy} \\ \varepsilon_{xy} \end{pmatrix} = \begin{bmatrix} \frac{1}{E} & -\frac{\nu}{E} & 0 \\ -\frac{\nu}{E} & \frac{1}{E} & 0 \\ 0 & 0 & \frac{1}{2G} \end{bmatrix} \begin{pmatrix} \sigma_{xx} \\ \sigma_{yy} \\ \sigma_{xy} \end{pmatrix}$$

We find $E = 56.18$, $\nu = 0.215$, and $G = 24.17$.

DOI: 10.1002/nme

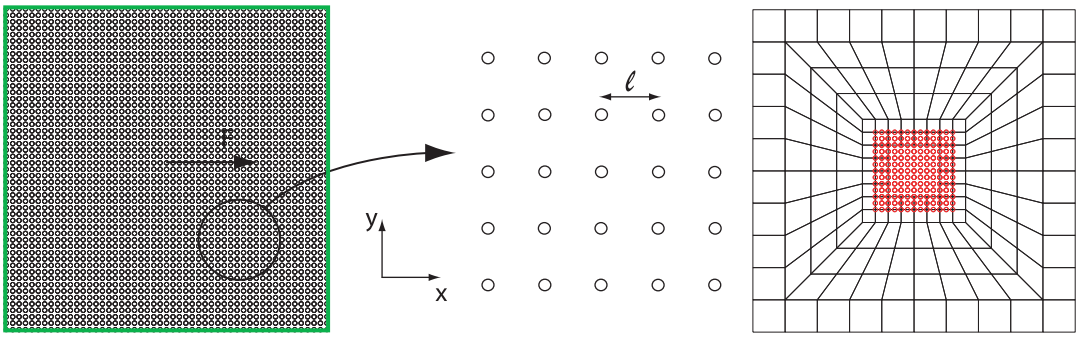

Figure 23. The 2D lattice defining the model problem (left) and the coupling model (right).

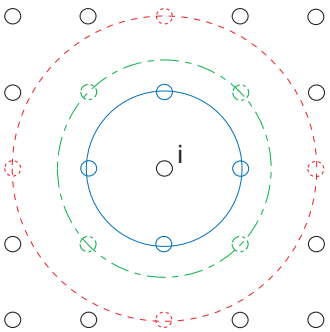

Figure 24. Interactions considered between particles: each particle i interacts with first (particles on solid line), second (particles on dash-dotted line), and third (particles on dash line) neighbors.

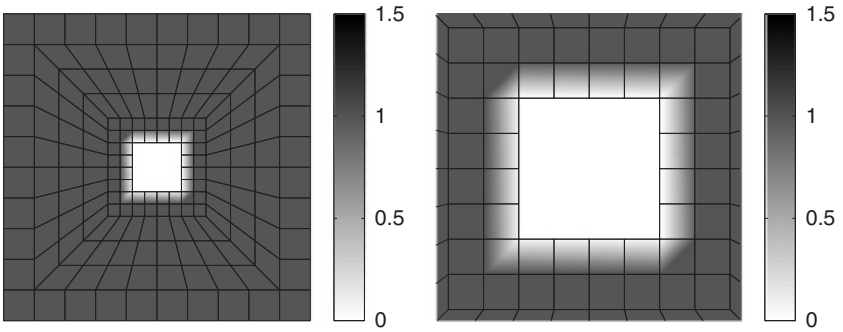

Figure 25. Representation of the piecewise linear weight function α^c. The picture on the right is a zoom around Ω_a.

The loading $\mathbf{F}$ is applied in 10 increments of magnitude $dF = 0.1$. This loading enables us to remain in the linear elasticity regime in Ω_c. In the overlap region Ω_o, the concurrent models are coupled using a coupling term based on the H^1-norm (15). The Lagrange multiplier is discretized on the finite element mesh used in Ω_c; the mesh is made of quadrilateral elements of size $2\ell \times 2\ell$. Finally, the weight function $\alpha^c(x, y)$ is chosen as piecewise linear on Ω_o (see Figure 25).

DOI: 10.1002/nme

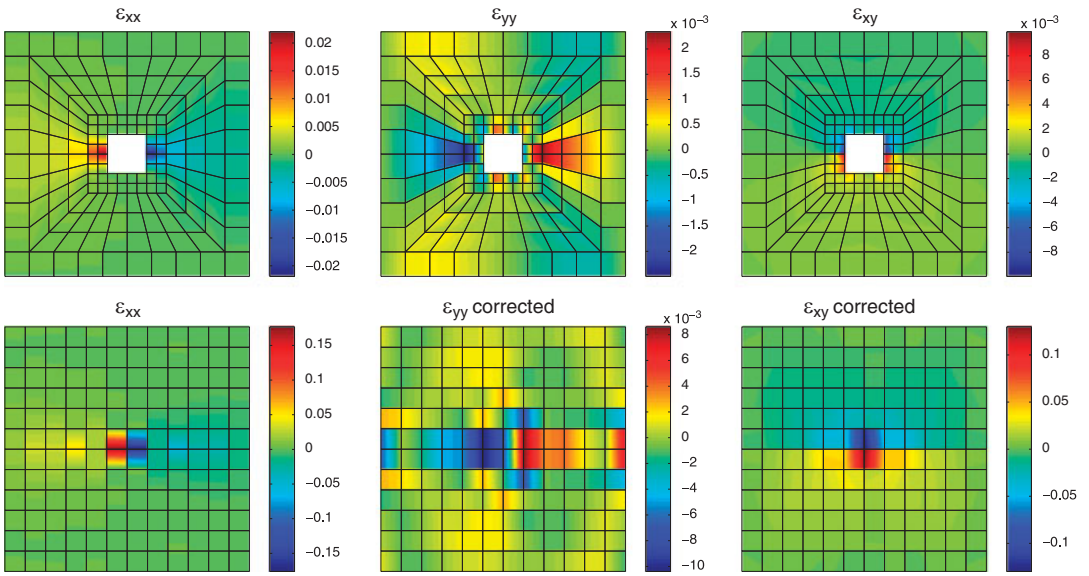

Figure 26. Strain field in the continuum region Ω_c (top) and in the particle region Ω_a (bottom).

The resulting nonlinear problem is solved by means of the Newton method and the strain fields associated with the continuum and particle models, in Ω_c and Ω_a respectively, are shown in Figure 26. For the particle model, the 'strain field' is computed by constructing a continuous displacement based on the linear interpolation of the particle displacements. We clearly observe the spurious effects in the neighborhood of the coupling region Ω_o, these being due to the same sources as those described in Section 4 (namely free modes and long–range interactions).

The spurious effects are corrected here by introducing dead forces using one layer of phantom particles. The dead forces, computed after the first iteration and weighted by the coefficients α^c and α^a, are shown in Figure 27. The discrete values of the forces, defined at nodes and particles, are actually interpolated over Ω_c and Ω_a. We observe that these weighted dead forces are non-zero only in a local neighborhood of the overlap region Ω_o. Five iterations were necessary to converge to the final corrected strain field, during which the dead forces were reduced of about two orders of magnitude. The final weighted dead forces and corrected strain fields (i.e. after five iterations of the correcting process) are shown in Figures 28 and 29, respectively. Some localized effects, which slightly perturb the solution, can however still be observed in the particle region, in particular in the vicinity of the overlap boundary where α^a is very small. This is due to the fact that the dead forces applied to the particles in this region have limited influence on the result. Nevertheless, convergence is improved when using a constant weight function α^c in Ω_o.

6.4. Comparison of performance between the corrective technique and a classical model adaptation procedure

In this last section, we compare the performance of the proposed correcting technique with that of an adaptive procedure consisting in enlarging the particle zone Ω_a up to a given error criterion [3, 13].

DOI: 10.1002/nme

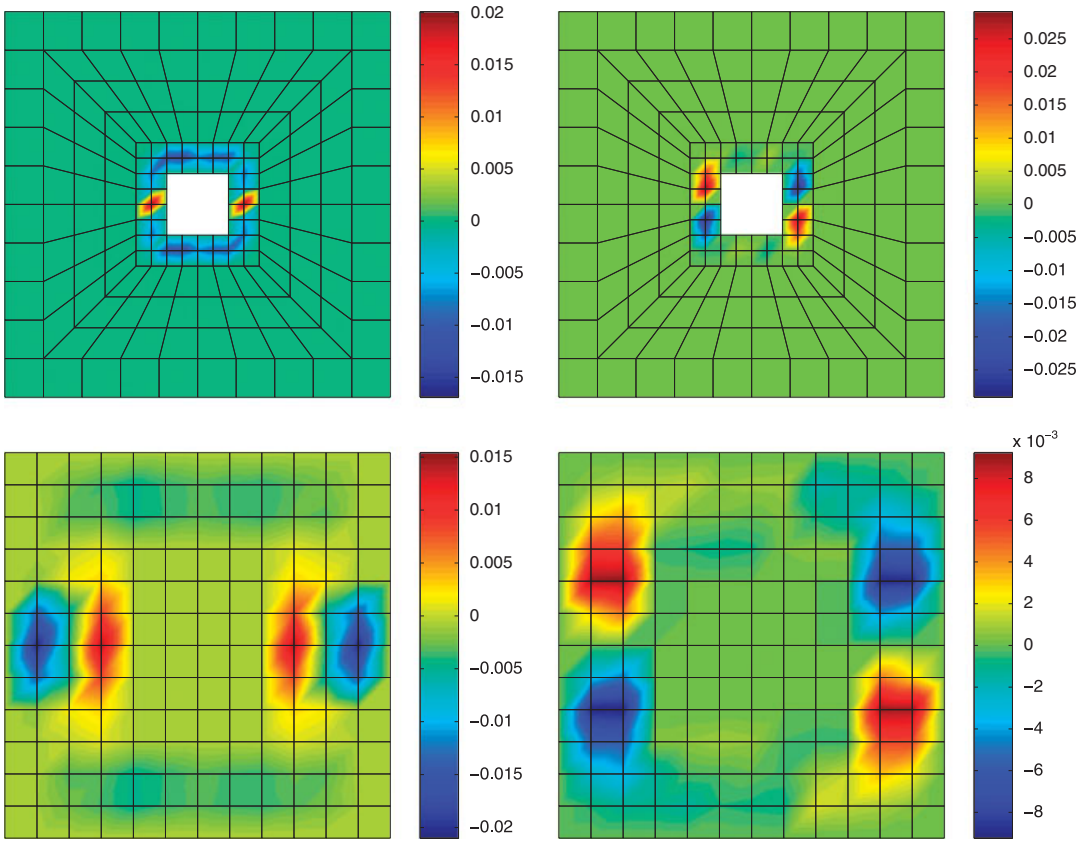

Figure 27. Interpolation map of the weighted dead forces applied at nodes in Ω_c (top) and at particles in Ω_a (bottom) at iteration 1. The x component (resp. y component) of the dead forces is represented on the left (resp. right).

In the latter approach, the idea is to ignore the spurious effects and to simply design optimal Arlequin configurations with respect to local quantities of interest.

We consider here a one-dimensional particle structure Ω, made of $N_p = 171$ particles, with $\ell = 0.2$. Particles interact with nearest and next-nearest neighbors. We assume that the structure Ω is fixed on its left and right end points and that it is subjected to a pointwise force F applied to the central particle P (see Figure 30). Furthermore, we suppose that the structure is subjected to a local defect that affects several particles around particle P; the defect is applied by weakening the stiffness coefficient of the corresponding bonds, i.e. by changing the initial stiffness k_i ($i = 1$ or 2) of these bonds to k_i^* such that:

$$\frac{k_i^*}{k_i} = \frac{1}{1+\kappa(\bar{x})}, \quad \bar{x} = \frac{x_{b_1} + x_{b_2}}{2} \tag{30}$$

where particles b_1 and b_2 denote the two particles involved in a given bond. The function κ is chosen as $\kappa(x) = 10\mathrm{e}^{-2x^2}$ so that about 20 particles are involved in the defect (see Figure 31).

DOI: 10.1002/nme

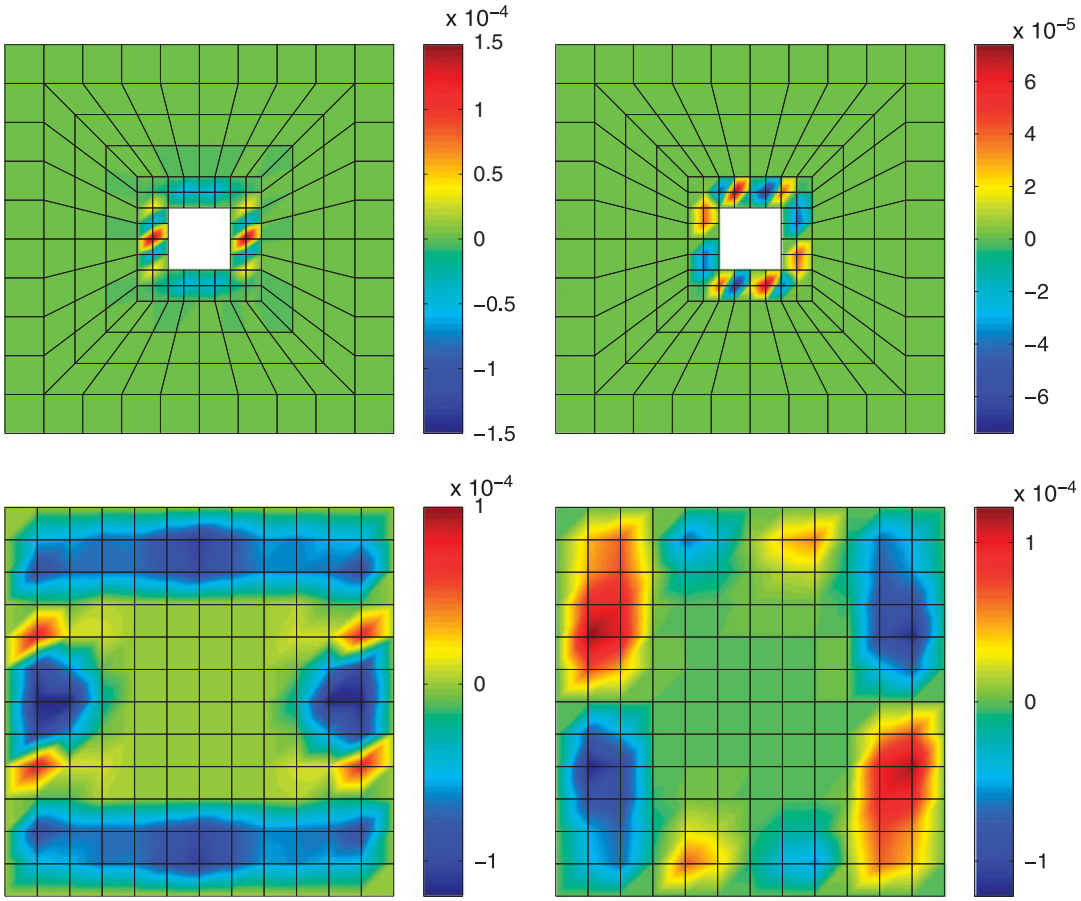

Figure 28. Interpolation map of the weighted dead forces applied at nodes in Ω_c (top) and at particles in Ω_a (bottom) at iteration 5. The x component (resp. y component) of the dead forces is represented on the left (resp. right).

The objective of the computation is to assess the value of two specific quantities of interest, namely the horizontal displacement of particle P, $Q_1 = z_P$, and the stretching of the bond between particle P and particle $P-1$, $Q_2 = (z_P - z_{P-1})/\ell$. We use the molecular model in a small region Ω_a around the central particle P and replace the remainder of the structure by a linear elastic material with equivalent Young's modulus E^{eq}. We set the size of the two overlap regions equal to 8ℓ and discretize the continuum and overlap regions by means of a finite element mesh with characteristic size $h_e = 4\ell$ (i.e. $s_e = 4$), as shown in Figure 32. Moreover, the weight function $\alpha_c(x)$ is chosen linear in the two overlap regions.

In the first numerical experiment, we set $k_1 = 100$ and $k_2 = 0$ so that particles interact with nearest neighbors only. We compare the approximate values of Q_1 and Q_2 obtained with or without using the correcting technique in the Arlequin coupling as a function of the size of the particle region Ω_a, more precisely the size of $\Omega_a^* = \Omega_a/(\Omega_a \cap \Omega_c)$. The reference values are $Q_1^{\text{ref}} = 0.5816642672$

DOI: 10.1002/nme

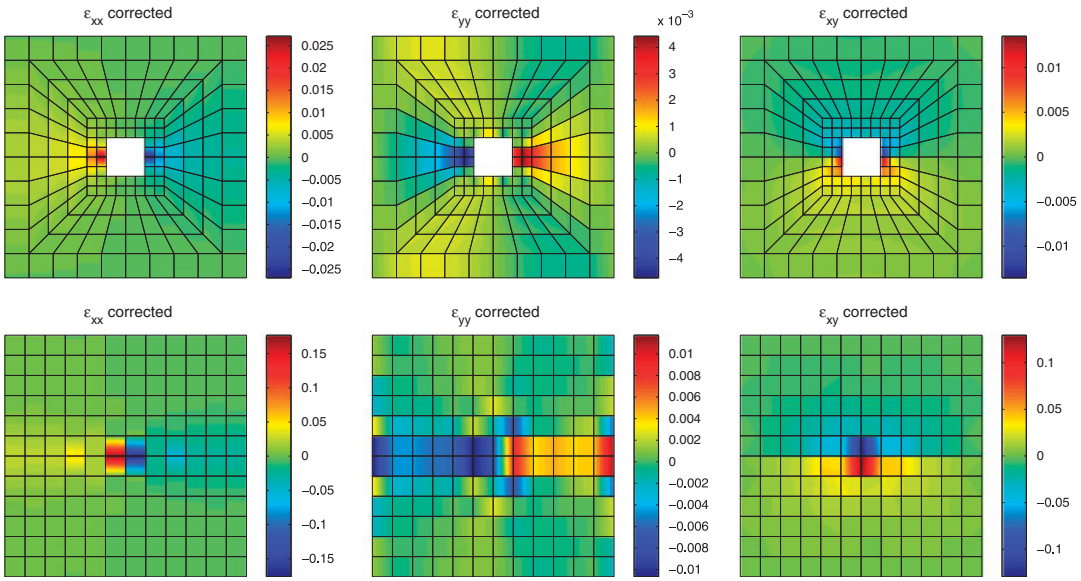

Figure 29. Corrected strain field in the continuum region Ω_c (top) and in the particle region Ω_a (bottom) at iteration 5.

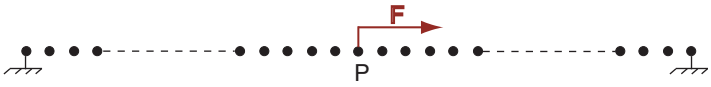

Figure 30. The 1D structure being considered.

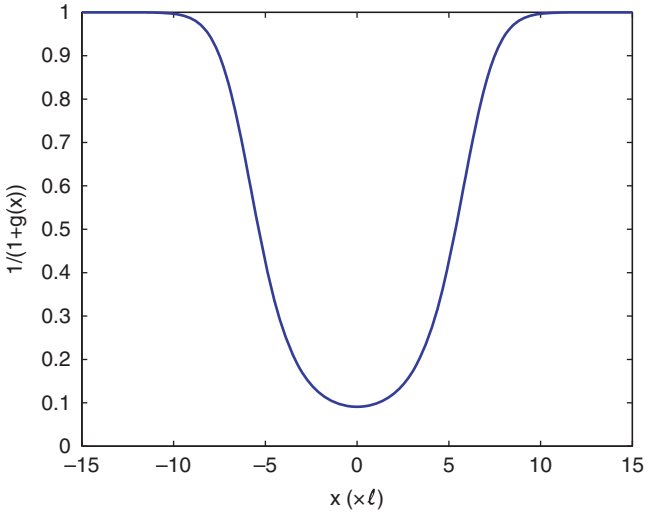

Figure 31. Function used to simulate a defect in the middle of the structure.

DOI: 10.1002/nme

Figure 32. Coupling between the particle and the continuum model in the Arlequin framework.

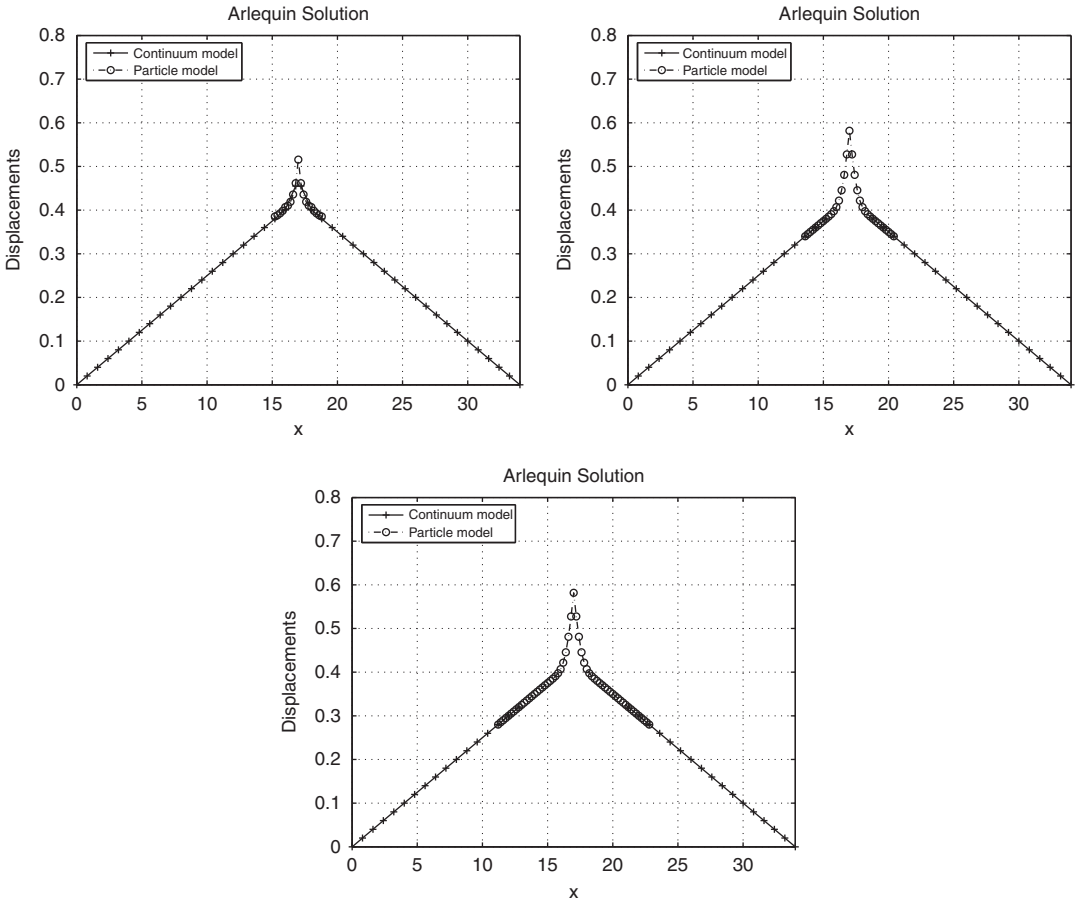

Figure 33. Approximate displacement solutions obtained using the Arlequin framework with various sizes of Ω_a^*: 2ℓ (top left), 18ℓ (top right), and 42ℓ (bottom).

and $Q_2^{\text{ref}} = 0.27$. Figure 33 shows the Arlequin solution in the cases Ω_a^* equal to 2ℓ, 18ℓ, or 42ℓ and Table II reports the relative error using the Arlequin method, first without any correction, and then using the corrective method after 5 and 10 iterations.

In the second series of experiments, we set $k_1 = 100$ and $k_2 = 50$ so that particles interact with nearest and next-nearest neighbors. Keeping the same configuration as in the previous study, the new results are reported in Table III. The new reference values are $Q_1^{\text{ref}} = 0.2042171911$ and $Q_2^{\text{ref}} = 0.1549328420$. Let us point out that in this case the reference values are not the ones given by a fully atomistic computation but the ones given by an Arlequin coupled solution obtained on

DOI: 10.1002/nme

Table II. Relative error on the values of Q_1 and Q_2 with respect to the size of Ω_a^* when using the Arlequin coupling with or without the corrective method.

Size of $\Omega_a^*(\times\ell)$	Relative error for Q_1 (%)			Relative error for Q_2 (%)		
	No correct.	Cor. (5 iter.)	Cor. (10 iter.)	No correct.	Cor. (5 iter.)	Cor. (10 iter.)
2	11.34	2.76	1.17	0	0	0
10	0.22	8.38×10^{-3}	2.79×10^{-4}	0	0	0
18	7.19×10^{-4}	5.41×10^{-7}	6.13×10^{-8}	0	0	0
26	3.44×10^{-7}	9.91×10^{-9}	7.79×10^{-10}	0	0	0
34	2.96×10^{-9}	2.14×10^{-10}	1.22×10^{-10}	0	0	0
42	8.32×10^{-10}	9.04×10^{-11}	2.37×10^{-11}	0	0	0

Table III. Relative error on the values of Q_1 and Q_2 with respect to the size of Ω_a^* when using the Arlequin coupling with or without the corrective method.

Size of $\Omega_a^*(\times\ell)$	Relative error for Q_1 (%)			Relative error for Q_2 (%)		
	No correct.	Cor. (5 iter.)	Cor. (10 iter.)	No correct.	Cor. (5 iter.)	Cor. (10 iter.)
2	8.72	1.14	0.26	11.66	2.12	0.97
10	0.14	5.99×10^{-4}	2.22×10^{-5}	7.80×10^{-3}	6.14×10^{-5}	9.37×10^{-6}
18	3.51×10^{-5}	9.11×10^{-7}	1.33×10^{-7}	1.48×10^{-5}	4.51×10^{-8}	1.19×10^{-8}
26	3.92×10^{-7}	7.40×10^{-9}	1.12×10^{-9}	7.47×10^{-8}	8.33×10^{-9}	2.26×10^{-10}
34	9.11×10^{-9}	8.26×10^{-10}	4.52×10^{-10}	6.77×10^{-9}	4.44×10^{-10}	8.21×10^{-11}
42	1.56×10^{-10}	8.84×10^{-11}	3.13×10^{-11}	2.94×10^{-10}	7.37×10^{-11}	9.16×10^{-12}

a sufficiently large Ω_a^* and using the correction technique with 20 iterations. The reason is that the two methods would provide different values as an error is made close to the boundaries when using a nonlocal particle model (long-range interactions) while keeping a local continuum model in the coupling. A way to avoid this boundary effect would consist of using a nonlocal constitutive relation for the continuum model.

We conclude from these experiments that the correction technique definitely has a positive effect on the accuracy of the quantities of interest Q_1 and Q_2 in the sense that a smaller atomic region is necessary to reach the same accuracy when using our corrective method. We also remark that depending on the choice of the quantity of interest, the corresponding relative error due to the spurious effects may be large, negligible, or even zero. However, depending on the computational cost and prescribed accuracy tolerance, it may be more effective to simply enlarge the particle region Ω_a rather than to use the correction technique. A compromise should then be made between computational cost and accuracy.

7. CONCLUSION

We have presented in this paper a technique for correcting spurious effects that arise in solutions of the Arlequin coupling method. It involves computing dead forces, obtained from a relatively

DOI: 10.1002/nme

inexpensive post-processing of the approximate solution, and injecting these into the coupling formulation in order to counterbalance the non-physical effects. As dead forces depend on the approximate solution, the procedure takes the relaxation effects into account through an iterative process. The corrective technique is similar to the one developed for the quasi-continuum method, but in our case, the dead forces are introduced into the formulation by means of a partition of unity. Furthermore, the use of the corrective method does not lessen the flexibility of the Arlequin approach, which in the case of atomic and continuum coupling does not require the use of the Cauchy–Born hypothesis. Results obtained from several 1D and 2D examples confirm that the corrective technique is effective in the sense that the approximate solution now converges to the physical solution, free of spurious effects, provided that the coupling parameters are consistent.

ACKNOWLEDGEMENTS

The support of this work by the U.S. Department of Energy within its multiscale mathematics program under contract DE-FG02-05ER25701 is gratefully acknowledged.

REFERENCES

1. Liu WK, Karpov EG, Zhang S, Park HS. An introduction to computational nanomechanics and materials. *Computer Methods in Applied Mechanics and Engineering* 2004; **193**:1529–1578.
2. Fish J. Bridging the scales in nano engineering and science. *Journal of Nanoparticle Research* 2006; **8**(6):577–594.
3. Bauman PT, Oden JT, Prudhomme S. Adaptive multiscale modeling of polymeric materials: Arlequin coupling and goals algorithm. *Computer Methods in Applied Mechanics and Engineering* 2009; **198**:799–818.
4. Fish J, Nuggehally MA, Shephard MS, Picu CR, Badia S, Parks ML, Gunzburger M. Concurrent AtC coupling based on a blend of the continuum stress and the atomic force. *Computer Methods in Applied Mechanics and Engineering* 2007; **196**:4548–4560.
5. Broughton JQ, Abraham FF, Bernstein N, Kaxiras E. Concurrent coupling of length scales: methodology and application. *Physical Review B* 1999; **60**(4):2391–2403.
6. Wagner GJ, Liu WK. Coupling of atomistic and continuum simulations using a bridging scale decomposition. *Journal of Computational Physics* 2003; **190**(1):249–274.
7. Xiao SP, Belytschko T. A bridging domain method for coupling continua with molecular dynamics. *Computer Methods in Applied Mechanics and Engineering* 2004; **193**:1645–1669.
8. Ben Dhia H. Multiscale mechanical problems: the Arlequin method. *Comptes Rendus de l'Académie des Sciences*, *Paris*, *Série II B* 1998; **326**(12):899–904.
9. Tadmor EB, Ortiz M, Phillips R. Quasicontinuum analysis of defects in solids. *Philosophical Magazine* 1996; **A73**:1529–1563.
10. Shilkrot LE, Miller RE, Curtin WA. Coupled atomistic and discrete dislocation plasticity. *Physical Review Letters* 2002; **89**:025501.
11. Bauman PT, Ben Dhia H, Elkhodja N, Oden JT, Prudhomme S. On the application of the Arlequin method to the coupling of particle and continuum models. *Computational Mechanics* 2008; **42**:511–530.
12. Ben Dhia H, Elkhodja N. Coupling of atomistic and continuum models in the Arlequin framework. *Proceedings of Congrès de Mécanique*, El Jadida, Maroc, 2007; 133–135.
13. Prudhomme S, Chamoin L, Ben Dhia H, Bauman P. An adaptive strategy for the control of modeling error in two-dimensional atomic-to-continuum coupling simulations. *Computer Methods in Applied Mechanics and Engineering* 2009; **198**:1887–1901.
14. Chamoin L, Oden JT, Prudhomme S. A stochastic coupling method for atomistic-to-continuum Monte-Carlo simulations. *Computer Methods in Applied Mechanics and Engineering* 2008; **197**(43–44):3530–3546.
15. Ben Dhia H. Further insights by theoretical investigations of the multiscale Arlequin method. *Multiscale Computational Engineering* 2008; **6**(3):215–232.
16. Xu M, Gracie R, Belytschko T. A continuum-to-atomistic bridging domain method for composite lattices. *International Journal for Numerical Methods in Engineering* 2009; **81**(13):1635–1658.

DOI: 10.1002/nme

17. Shenoy VB, Miller RE, Tadmor EB, Rodney D, Phillips R, Ortiz M. An adaptive finite element approach to atomic-scale mechanics: the quasicontinuum method. *Journal of the Mechanics and Physics of Solids* 1999; **47**:611–642.
18. Knap J, Ortiz M. An analysis of the quasicontinuum method. *Journal of the Mechanics and Physics of Solids* 2001; **49**:1899–1923.
19. Miller RE, Tadmor EB. The quasicontinuum method: overview, applications and current directions. *Journal of Computer-Aided Materials Design* 2002; **9**:203–239.
20. Curtin WA, Miller RE. Atomistic/continuum coupling in computational material science. *Modeling and Simulation in Materials Science and Engineering* 2003; **11**:R33–R68.
21. Badia S, Bochev P, Fish J, Gunzburger M, Lehoucq R, Nuggehally M, Parks M. A force-based blending model for atomistic-to-continuum coupling. *International Journal for Multiscale Computational Engineering* 2007; **5**:387–406.
22. Badia S, Parks M, Bochev P, Gunzburger M, Lehoucq R. On atomistic-to-continuum (atc) coupling by blending. *SIAM Journal on Multiscale Modeling and Simulation* 2008; **7**(1):381–406.
23. Ben Dhia H, Rateau G. The Arlequin method as a flexible engineering design tool. *International Journal for Numerical Methods in Engineering* 2005; **62**(11):1442–1462.
24. Ben Dhia H, Rateau G. Analyse mathématique de la méthode Arlequin mixte. *Comptes Rendus de l'Académie des Sciences*, *Paris*, *Série I* 2001; **332**:649–654.
25. Guidault PA, Belytschko T. On the L^2 and the H^1 couplings for an overlapping domain decomposition method using Lagrange multipliers. *International Journal for Numerical Methods in Engineering* 2007; **70**(3):322–350.
26. Dobson M, Luskin M. An analysis of the effect of ghost force oscillation on quasicontinuum error. M2AN *Mathematical Modeling and Numerical Analysis* 2009; **43**(3):591–604.
27. Zhang S, Khare R, Lu Q, Belytschko T. A bridging domain and strain computation method for coupled atomistic-continuum modelling of solids. *International Journal for Numerical Methods in Engineering* 2007; **70**:913–933.

DOI: 10.1002/nme